GEM NEWS INTERNATIONAL

Contributing Editors

Gagan Choudhary, *IIGJ-Research & Laboratories Centre, Jaipur, India* (gagan.choudhary@iigjrlc.org)

Christopher M. Breeding, *GIA, Carlsbad* (christopher.breeding@gia.edu)

Guanghai Shi, *School of Gemmology, China University of Geosciences, Beijing* (shigh@cugb.edu.cn)

TUCSON 2023

This year's Tucson shows were well attended, and many vendors were relieved by the strong sales. In fact, the only "complaint" from vendors this year was that for many it was too busy to take even a short break away from their booths. Some vendors reported selling less than in 2022, but still more than in pre-COVID years.

Supply chain issues resulting from lack of output during the pandemic are still being felt. For many sellers demand often exceeded supply, especially for fine-quality colored stones, and prices are increasing to reflect that. With this increase expected to continue, the heavy booth traffic could be due to consumers buying as much as possible at these price points. This corresponds with comments from Nathan Renfro on the GIA show services laboratory, which received a near-record number of submissions this year. As for the trends in materials submitted to the lab, he indicated a typical mix of the major stones: mainly ruby, sapphire, emerald, Paraíba tourmaline, and alexandrite.

At the AGTA GemFair and Gem & Jewelry Exchange (GJX) shows, sapphire, large freshwater pearls from China, and Ethiopian opal were among the eye-catching gems. Sapphire was once again a top seller, with blue and untreated colors doing especially well. Many fancy-color sapphires, including ones in saturated hues such as magenta, were available (Pantone's Color of the Year for 2023 is Viva Magenta) (figure 1). There were multiple sellers of akoya, Tahitian, and "Edison" pearls in both venues. Most notably, "Edison" pearls were available in much larger sizes and with more saturated colors than in years past (figure 2). Non-nacreous pearls were also featured more prominently. Ethiopian opal, first introduced in Tucson in 2009, was very popular this year. It has climbed from a novelty to a gemstone found in top designer luxury jewels, such as the Zoltan David necklace shown on the cover of this issue and the pin featuring both Ethiopian opal and conch pearls

Figure 1. This ring from Graff features a 3.95 ct pink sapphire and 7.5 carats of diamond in a spiral design. Photo by Robert Weldon; courtesy of Jewelerette Co.

Editors' note: Interested contributors should send information and illustrations to Stuart Overlin at soverlin@gia.edu.

Banner photo of Afghan kunzite by Robert Weldon; courtesy of Dudley Blauwet, Mountain Minerals International.

Gems & Gemology, Vol. 59, No. 1, pp. 102–162.

Figure 2. Left: "Edison" pearls were available in large sizes and attractive colors. Photo by Si Athena Chen; courtesy of A&B Jewelry. Right: A strand of "Edison" pearls of various colors, in sizes from 14 to 16 mm. Photo by Mimi Travis; courtesy of Yen's Jewelry & Accessories.

in figure 3. Tourmaline from newly discovered pockets in San Diego County's Pala District was also on display.

Figure 3. This pin features a 63.92 ct Ethiopian opal with 23.85 carats of conch pearl, 5.88 carats of natural pearl, and 15.85 carats of diamond, set in platinum. Photo by Robert Weldon; courtesy of Pioneer Gems of New York.

The demand for one-of-a-kind gems was apparent in all aspects—cut, color, and even inclusions. Nontraditional cuts such as slices, fantasy cuts, rose cuts, kites, and tablets were readily found in gems ranging from rutilated quartz to diamond (figure 4). Beyond nonstandard cuts, stones

Figure 4. Earrings featuring diamond slices and rose-cut rubies. Photo by Mimi Travis.

Figure 5. "Salt and pepper" diamonds containing eye-visible inclusions. Photo by Jennifer Stone-Sundberg; courtesy of Misfit Diamonds.

with obvious inclusions were very popular. The appeal of these stones centers on their uniqueness. "Salt and pepper" diamonds with multiple eye-visible white, gray, and black inclusions were available loose (figure 5) and in jewelry items throughout the shows. Similarly, nontraditional colors for particular varieties, including color-change stones, pastel colors (such as "mint" tourmaline), teal, and bicolor stones, were trending (figure 6). Strong demand for these nontraditional or one-of-a-kind stones comes from small-scale individual designers with the ability to promote to a wide audience via social media.

In 2020, we reported on the first Ethical Gem Fair in Tucson. This year, suppliers at the fair were pleasantly surprised by the number of large jewelry manufacturers who attended for the first time. The trend toward responsible sourcing, traceability, transparency in practices, and social awareness, which has long been a key differentiator for some jewelers, is clearly becoming more mainstream as customers increasingly demand to know more about the origin and impact of the stones they are purchasing. This year, jewelers at AGTA and GJX also emphasized the importance of providing an environmentally conscious product and the increasing demand from clients for full chain-of-custody information on stones. Similarly, many small-scale designers and buyers were seeking out gems mined in the United States, such as Montana sapphire, Oregon sunstone, and amethyst from the Four Peaks mine in Arizona. They noted high demand for these gems, which seem to satisfy consumer sustainability concerns. In many cases, the younger generation of jewelers has brought a focus on ethical and environmentally sound practices to multigenerational businesses.

We hope you enjoy our coverage of the 2023 Tucson gem shows, where you'll find striking pieces we saw, the latest trends, mining updates, and more.

The following contributed to this report: Lisa Neely, Mimi Travis, Nathan Renfro, Albert Salvato, and Wim Vertriest.

Jennifer Stone-Sundberg, Si Athena Chen, Lisa Kennedy, Robert Weldon, and Erin Hogarth

COLORED STONES AND ORGANIC MATERIALS

Enormous cat's-eye aquamarine. On the AGTA show's opening day, we were on hand as Gary Bowersox and Kathleen Kolt-Bowersox donated an extraordinary cat's-eye aquamarine to Dr. Jeffrey Post, mineralogist and curator-in-charge of gems and minerals at the Smithsonian National Museum of Natural History (figure 7).

The 586.43 ct untreated transparent light greenish blue aquamarine with a sharp cat's-eye is from the Pech Valley pegmatite mine in Afghanistan. The rough (figure 8, left) weighed approximately 7,700 ct and was kept for 15 years

Figure 6. An unusual 6.95 ct cushion-cut bicolor alexandrite from Madagascar displaying a color change from yellowish green and reddish brown in daylight (left) to yellowish orange and orangy brown in incandescent illumination (right). Photos by Robert Weldon; courtesy of Bryan Lichtenstein, 3090 Gems, LLC.

Figure 7. Left: A 586.43 ct cat's-eye aquamarine donated by Gary Bowersox and Kathleen Kolt-Bowersox to the Smithsonian National Museum of Natural History gem collection. Photo by Robert Weldon; courtesy of the Smithsonian National Museum of Natural History. Right: Dr. Jeffrey Post (left) and Gary Bowersox with the cat's-eye aquamarine. Photo by Kathleen Kolt-Bowersox.

before it was finally cut in 2017 by Rohitha Perera in Sri Lanka (figure 8, right). The Bowersoxes have several other cut gems from this find, with the next largest weighing in at 541.96 ct.

Jennifer Stone-Sundberg and Si Athena Chen
GIA, Carlsbad

New violet orbicular chalcedony from Ethiopia. At the GJX show, the author encountered a relatively new find of violet chalcedony reportedly discovered in Ethiopia in 2019 (figure 9). Processed and brought to market as tumble-polished freeforms, the chalcedony was offered by Orbit Ethiopia Plc. According to managing director Tewodros Sintayehu, the mine is located in the Gamo Zone region, approximately 600 km from Addis Ababa. The material was first discovered in the Gerese District and has since been found in the adjacent districts of Kamba and Garda Marta. Sintayehu noted that he had a very large quantity of the material stockpiled.

The notable features of this material were its fairly vivid violet color as well as the multitude of white orbicular struc-

Figure 8. Left: Kathleen Kolt-Bowersox holding the 7,700 ct aquamarine rough before it was cut. Right: The rough aquamarine was cut and polished in Sri Lanka by Rohitha Perera. Photos by Gary Bowersox.

Figure 9. This relatively new type of violet chalcedony from Ethiopia (here, 75–198 ct) displays a wonderful pattern of white orbs. Photo by Annie Haynes; courtesy of Orbit Ethiopia Plc.

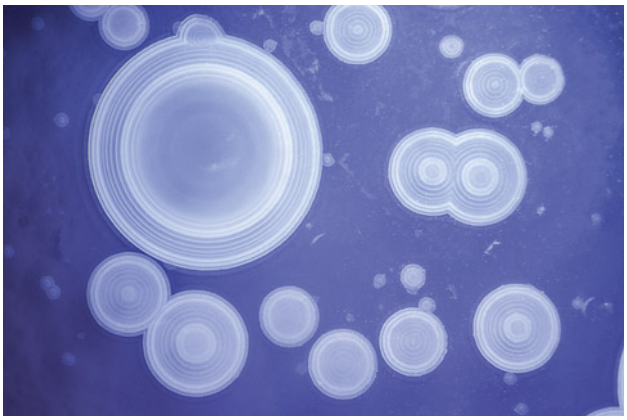

Figure 10. White orb-like structures were confined to a shallow surface layer in the violet chalcedony from Ethiopia. Photomicrograph by Nathan Renfro; field of view 15.16 mm.

tures distributed across the surface of the gems (figure 10). Microscopic examination revealed that the white color was related to a distinct botryoidal structure where a shallow outer layer of the gems contained all of the white areas. Because the white orbs are confined to a shallow surface layer, this explains why the material was sold as tumble-polished nuggets: Cutting the material into cabochons would likely result in the loss of the white orbicular pattern. A few unidentified mineral inclusions were also observed with the microscope, but the cause of the outer layer's white orb pattern remains unclear.

This new material is quite remarkable for its beautiful pattern. Even if it is only made available as freeform tumble-polished stones, it will be a welcome addition to the chalcedony market.

Nathan Renfro
GIA, Carlsbad

Italian precious coral. Coral from the Mediterranean Sea has been harvested and used for adornments for thousands of years. More than 7,000 species are categorized as precious, common, or reef coral. Precious coral is defined by the World Jewellery Confederation (CIBJO) Coral Commission as "those that are used in jewelry and decoration, specifically red, pink, and white varieties with porcelain-like luster after polishing." Italian coral harvested from the *Corallium rubrum* species is considered precious.

At the GJX show, the authors spoke with Sergio Di Gennaro of Fulvio Di Gennaro Srl. (Torre del Greco, Naples) about the Italian coral market. The Mediterranean has been precious coral's major source since it was first collected for ornamentation over 3,000 years ago, followed by Taiwan and Japan with smaller quantities. Beginning in the late 1970s, Mediterranean coral was threatened by overharvesting. Di Gennaro explained that many strict regulations for harvesting coral are in place today. Harvesting is limited to coral with trunks having a basal diameter of at least 7 mm recovered from 50 meters or deeper by licensed scuba divers.

Precious coral is the exoskeleton of very tiny marine invertebrates, known as coral polyps. When a colony of polyps arrives in a particular area, they start to create the exoskeletons on rocks, growing upward in a branch-like or fan formation. Di Gennaro mentioned that divers do not harvest coral with active colonies as these will continue to grow and the future, larger coral will be more valuable. Divers therefore tend to harvest the coral where the colony has already left. Unlike other types of corals, such as common and reef, these Mediterranean "deep sea" precious corals are not a natural habitat for other marine species. Reef coral species, which are a natural environment to many different marine species, are in many cases endangered and must be preserved.

Di Gennaro explained that the quality of the coral depends on the locality. He showed us a piece of dark red coral (figure 11, left), which is the typical color of coral harvested from northern Sardinia. It is a darker red due to cooler water temperatures from strong currents in the area. Coral from the southern portion of Sardinia (figure 11, center) tends to be lighter in color. Di Gennaro described this as a more "classic" color of Mediterranean coral. He also showed us a piece of reddish orange coral called "Sciacca," named for a town in southern Sicily where the coral is harvested (figure 11, right). Di Gennaro said that volcanic activity below the surface results in warmer water temperatures, which in turn causes a more orangy color.

Di Gennaro emphasized the importance of sustainability in the coral industry, noting the heritage of the city of Torre del Greco, which was built on the art of processing coral. While current restrictions have reduced the amount of coral

Figure 11. Mediterranean coral from different regions. Left: Dark red fine coral from the northern coast of Sardinia. Center two pieces: "Classic" coral from the southern coast of Sardinia. Right: Orangy coral, termed "Sciacca," from the coast of southern Sicily. Photo by Lisa Kennedy; courtesy of Fulvio Di Gennaro Srl.

being harvested compared to decades past, sustainable production will guarantee that we continue to see stunning Mediterranean precious coral for decades to come.

Lisa Kennedy and Cristiano Brigida
GIA, New York

Exceptional gemstone acquisitions by the Kreis family. Kreis Jewellery (Niederwörresbach, Germany) is known for master cutting expertise and distinctive jewelry design (see Spring 2022 GNI, pp. 86–87). At the GJX show, Stefan and Alexander Kreis showed us three recent gemstone acquisitions.

First was a 155 g aquamarine crystal containing a two-phase liquid and gas inclusion measuring 4.3 cm long (figure 12; see video at www.gia.edu/gems-gemology/spring-2023-gemnews-kreis-family-gemstones). The crystal was found in the 1960s in Marambaia, Minas Gerais, Brazil, and had been part of a private collection before the Kreises obtained it in 2022.

"It would even be a cuttable crystal," Alexander said. "Of course we would never touch it because of the specialty of the huge liquid inclusion. A liquid chamber that size in quartz would already be amazing," he continued. "But having it in an aquamarine, which is totally intact—you have the complete termination. And look at the sheer size of that crystal."

Marambaia was known for large quantities of aquamarine by 1900 and produced the 110.5 kg (244 lb), 552,500 ct Papamel, discovered in 1910, the largest known gem-quality aquamarine crystal. The crystal that was the basis for the Dom Pedro, the largest cut aquamarine, weighed around 45 kg (100 lb) and was also from Marambaia.

Stefan said they had received a 35.05 ct cat's-eye alexandrite (figure 13) that morning. He noted the size, exceptionally sharp eye, and superb color change for Sri Lankan alexandrite, which typically has a weaker color change than material from Russia and Brazil. Alexander pointed out that cat's-eyes are less common in alexandrite than in other chrysoberyl. "A cat's-eye alexandrite with a strong color change like this one is extraordinary," he said. "A size of 35 carats is what makes it outstanding."

Figure 12. A 155 g aquamarine crystal containing a liquid and gas bubble inclusion. The crystal measures 11.9 cm long and the inclusion 4.3 cm long. Photo by Robert Weldon; courtesy of Kreis Jewellery GmbH.

Figure 13. A 35.05 ct Sri Lankan cat's-eye alexandrite in daylight (left) and incandescent light (right). Photo by Robert Weldon; courtesy of Kreis Jewellery GmbH.

The Kreises also showed us a 7.08 ct padparadscha sapphire (figure 14). "The color mixture of this stone is a real padparadscha color," Stefan said. Alexander added that a range of colors fall into the padparadscha category, but "this is the perfect color."

The cat's-eye alexandrite and padparadscha sapphire will undoubtedly inspire exquisite jewelry designs from Sonja and Vanessa Kreis. Sonja noted, "It is a very intuitive process in which we try to bring out a gem's natural beauty in such a way that it blurs the boundaries between jewelry and art."

Erin Hogarth
GIA, Carlsbad

Rare double pseudomorph ikaite-calcite-opal. At the Pueblo Gem & Mineral Show, Graeme Dowton of Red Earth Opal (White Cliffs, Australia) exhibited rare double pseudomorph ikaite-calcite-opal gem specimens mined from the Naatji Nest mine at White Cliffs in New South Wales, Australia. Ikaite was initially substituted with calcite and then opalized, therefore making these double pseudomorph opals. Also called "pineapple opal" in the market due to the form of their clusters, they are found exclusively in White Cliffs and typically occur within weathering-bleached siltstones and claystones. According to Dowton, no other type of gem-quality opal was found in the same layer where the pineapple opals were mined. During mining, it was noticed that two opals had formed within a few feet of each other but with distinctly different coloration: One displayed a rich spectrum of play-of-color, while the other showed almost no coloration. The 3,510 ct Heart of Australia (figure 15) shows rich play-of-color and is considered one of the finest specimens of this type ever unearthed. In some of Dowton's samples, the precursor calcite was not fully substituted by silica gel, and white calcite crystals can be observed (figure 16).

Ikaite, $CaCO_3 \cdot 6H_2O$, is a rare and metastable hydrated carbonate in sedimentary rocks that has only been identified in environments ranging from –2° to 7°C in nature (M.L. Vickers et al., "The ikaite to calcite transformation: Implications for paleoclimate studies," *Geochimica et Cosmochimica Acta*, Vol. 334, 2022, pp. 201–216). The occurrence of ikaite suggests a period of very cold to near-freezing paleoclimate conditions in White Cliffs. At ambient

Figure 14. A 7.08 ct padparadscha sapphire. Photo by Robert Weldon; courtesy of Kreis Jewellery GmbH.

Figure 15. The Heart of Australia, a 3,510 ct double pseudomorph ikaite-calcite-opal gem specimen, is considered one of the finest ever unearthed. Courtesy of Graeme Dowton.

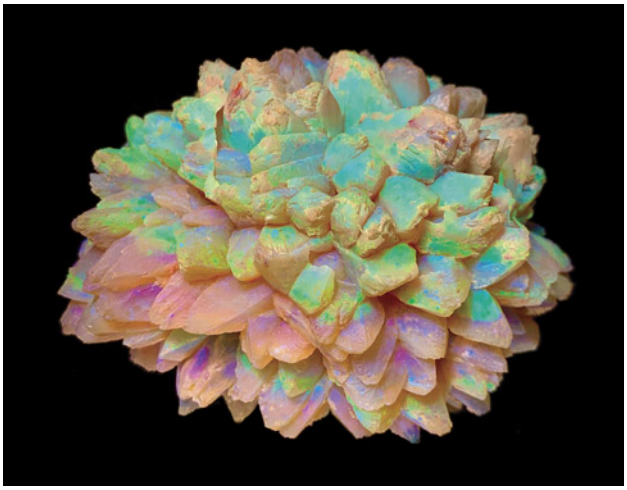

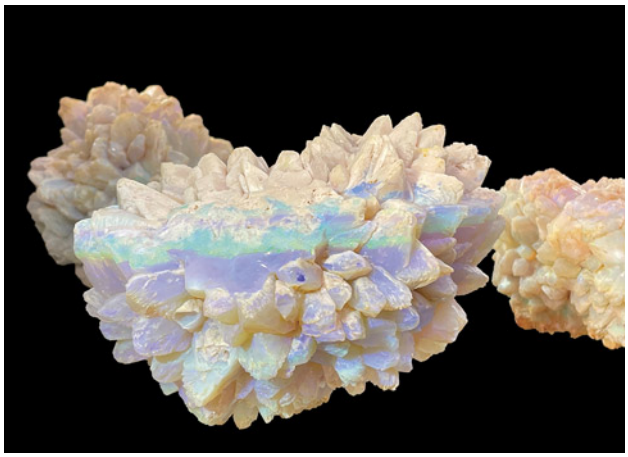

Figure 16. The intergrowth of opal and its precursor calcite in pineapple opal. This specimen is 12 × 10 × 8 cm and weighs 690 g. Photo by Si Athena Chen; courtesy of Graeme Dowton.

temperatures (10°–30°C), ikaite transforms to more stable carbonate polymorphs such as calcite, aragonite, and/or vaterite. The ikaite and its following pseudomorphs act as paleothermometers (D. Shearman and A. Smith, "Ikaite, the parent mineral of jarrowite-type pseudomorphs," *Proceedings of the Geologists Association*, Vol. 96, No. 4, 1985, pp. 305–314). When the host sedimentary rocks were weathered, they released silica into groundwater. This silica-bearing groundwater contacted with calcite, which gradually dissolved and reprecipitated to opal over time (B. Pewkliang et al., "The formation of precious opal: Clues from the opalization of bone," *Canadian Mineralogist*, Vol. 46, No. 1, 2008, pp. 139–149). However, the detailed formation mechanism of ikaite-calcite-opal in White Cliffs requires future investigation.

Si Athena Chen and Jennifer Stone-Sundberg

Cultured pearl market update. At the AGTA show, we spoke with several pearl dealers to acquire some insight into the current cultured pearl market. With demand for pearls trending upward in the secondary market, as reported by The Real Real in its Luxury Consignment Report in January 2023, it was easy to spot similar trends in other areas of the pearl market as well.

Bead cultured (BC) pearls are the result of the deliberate insertion of a bead nucleus along with a small piece of mantle tissue into the gonad of a living host mollusk to start the growth of the cultured pearl, a process known as nucleation or grafting. Non-bead cultured (NBC) pearls need only a piece of tissue implanted into the gonad or mantle of a host mollusk to form. A technique originally developed and successfully operated in Japan before adoption by other global operations including Australia, the Philippines, Indonesia, French Polynesia, and China, the nucleation process is intricate and requires expertly trained technicians.

The pearl industry, like others, was adversely affected by the COVID-19 pandemic. Many dealers noted a supply shortage of the main types of cultured pearls: South Sea, Tahitian, akoya, and freshwater. According to dealers, many pearl farms, especially Tahitian, use Chinese and Japanese technicians to perform the critical nucleation step. Due to travel restrictions and border closures during the pandemic, many experts were unable to travel to these locations, resulting in smaller harvests since 2020. In some farming areas, there were not enough employees on-site to keep the mollusks in good health, and thus the mortality rate was high. Assuming grafting returned to normal levels by 2022, a greater influx of supply is expected in 2024, given the typical 24-month growth periods. Some dealers added that strong demand for cultured pearls from Chinese and other Asian consumers is contributing to the current global shortage.

Small freshwater BC pearls from China (approximately 2–4 mm) were more widely available at the show than in past years, in near-round to round shapes and in various colors including white, pink, purple, and orange (figure 17). Freshwater cultured pearls of this particular size are typically NBC, normally oval (a potato-like shape), and can look similar to white saltwater Japanese akoya BC pearls of the same size. However, Gina Latendresse of American Pearl Company Inc. (Nashville, Tennessee) demonstrated

Figure 17. Near-round to round small freshwater bead cultured pearls (approximately 2–4 mm) were widely available at the AGTA show in various colors including white, pink, purple, and orange. Photo by Artitaya Homkrajae; courtesy of Betty Sue King, King's Ransom.

Figure 18. Left: Small round freshwater bead cultured (BC) pearls (top group of strands) and small round Japanese akoya BC pearls (bottom strands) appear very similar at first glance. Right: Upon closer inspection, the freshwater pearls more often show a rounded flat surface feature. Photos by Artitaya Homkrajae and Lisa Kennedy; courtesy of American Pearl Company Inc.

that upon closer inspection, the freshwater pearls more often show a rounded flat surface feature on an otherwise spherical pearl, a feature usually too small to affect basic shape (figure 18). This feature is also occasionally observed in other types of freshwater cultured pearls.

Eliko Pearl Company (New York City) displayed numerous strands of Vietnamese akoya BC pearls with bodycolors ranging from silver to light gray and light bluish gray with exceptional orient (figure 19). These provide a greater selection of colors compared to traditional akoya BC pearls. Some white, light cream, and cream pearls were also presented as unprocessed and untreated—steps normally used to improve appearance and alter color. However, many akoya BC pearls in the market have been processed to generate a classic white appearance. Vietnam has produced saltwater cultured pearls commercially since the 1990s and is expected to produce approximately 2,000 kg per annum (N. Sturman et al., "Vietnam: Shell nuclei, pearl hatcheries, and pearl farming," Fall 2020 *G&G*, pp. 402–415), which is significantly smaller than Japan's anticipated annual production of approximately 20 tons (roughly 18,000 kg) (T. Matsuyama et al., "Mass mortality of pearl oyster (*Pinctada fucata* (Gould)) in Japan in 2019 and 2020 is caused by an unidentified infectious agent," *PeerJ*, Vol. 9, 2021, article no. 12180).

Figure 19. Vietnamese akoya bead cultured pearls in various colors ranging from silver to light gray to light bluish gray. The pearls were said to be unprocessed and untreated. Photo by Lisa Kennedy; courtesy of Eliko Pearl Company.

Eric Yen of Yen's Jewelry & Accessories Inc. (San Francisco) and Alan Hakimian of Yoko London presented strands that combined multicolor pearls from different pearl types, offering variety and high fashion all at once (figures 20 and 21). Both pointed out that making mixed and graduated color strands is an efficient use of all the pearls produced from a harvest, just one example of economic sustainability in the pearl industry. Producing only perfectly matched color stands would lead to more waste.

Overall, pearl dealers are looking forward to the return of the gem, jewelry, and pearl shows in Hong Kong in 2023, as these are some of the largest shows for cultured pearls. Many have not been able to attend since 2019 due to lockdown restrictions in Hong Kong.

Lisa Kennedy
Artitaya Homkrajae
GIA, Carlsbad

"Edison" pearls: Increasing market presence. Several vendors at both the AGTA and GJX shows carried large and attractively colored "Edison" pearls from China (see C. Zhou

Figure 20. This set of ombré pearl strands, made up of round Tahitian pearls with silver and gold South Sea pearls ranging from 10 to 10.4 mm, is also known as shikisai*, which means "colors of four seasons" in Japanese. Photo by Mimi Travis; courtesy of Yen's Jewelry & Accessories Inc.*

Figure 21. Mixed strand of 79 pearls ranging from 11.8 to 14.8 mm, consisting of pink Chinese freshwater, black Tahitian, golden Indonesian, and white Australian bead cultured pearls. Also pictured is an exceptionally large 20.4 mm South Sea bead cultured pearl, weighing 12 g. Photo by Robert Weldon; courtesy of Yoko London.

et al., "Detection of color treatment and optical brightening in Chinese freshwater 'Edison' pearls," Summer 2021 *G&G*, pp. 124–134). These round freshwater bead cultured pearls generally ranged in size from 9 to 14 mm. Some baroque pearls were also offered. This year we saw deeper hues and more purple, bronze, copper, peach, and orangy pink colors than in the past; lighter colors such as white, cream, and light pink were more scarce. Popular trends included "rainbow" strands of pearls featuring a mix of colors, strands with alternating blocks of color, and strands with metallic colors (figure 22). At GJX, we spoke with Amy Hansen of A&B Jewelry (Honolulu, Hawaii) to learn about current purchasing trends and the latest developments at the pearl farms.

Hansen indicated that "Edison" pearls are still finding their place in the market. Her designer clients are seeking larger pearls, and those in the 12–14 mm size range are doing particularly well, with pearls larger than 13 mm in highest demand. She explained the limits in producing larger pearls: Larger sizes (particularly greater than 14 mm in diameter) take much more time to culture, which greatly limits the yield of top-grade product with respect to shape, nacre, surface, and luster. As a result, the highest-quality "Edison" pearls in sizes over 14 mm are rare and considerably more costly. That said, she noted that "Edison" pearls are still a good value, available in an appealing variety of colors and sizes with a price point substantially below akoya and Tahitian saltwater cultured pearls.

Hansen explained that the cultivation of "Edison" pearls in terms of bead size and culturing times is similar to that for saltwater Tahitian pearls. She described improvements in the process, including Chinese freshwater pearl farmers moving inland to access cleaner rivers and lakes and using more sound environmental practices. The move to these newer locations has resulted in more colors being achieved, broadening the offerings of these pearls. Chinese freshwater cultured pearl production has also decreased over the past five years as the focus has shifted

Figure 22. A graduated strand of "Edison" pearls in copper and bronze metallic colors, ranging from 9 to 12 mm. Also shown are three loose pearls: 10 mm peach, 11 mm purple, and 11 mm copper. Photo by Robert Weldon.

more to quality over quantity. The wholesale price of fine-quality "Edison" pearls is still considerably below that of similarly sized Tahitian and akoya pearls, but we expect the price gap to narrow somewhat as the quality and popularity of these beautiful freshwater cultured pearls continues to increase.

Jennifer Stone-Sundberg and Si Athena Chen

Spotlight on natural nacreous pearls. A natural pearl forms in the interior of a mollusk within a naturally formed pearl sac without human intervention. The use of natural pearls goes back thousands of years, and these biogenic gem materials have been treasured in jewelry and adornment throughout human history. In general, pearls can be separated into two varieties based on surface structure: nacreous and non-nacreous. The nacreous pearls are more common in the market. These are formed by a layered structure of aragonite platelets together with organic substances as well as water, and they normally display a pearly luster.

At the AGTA show, Alex Vock of ProVockative Gems Inc. (New York City) shared some of his expertise in natural saltwater nacreous pearls. With more than 30 years in the business, he is considered an industry leader specializing in signed collectible jewelry, natural gemstones, and natural pearls. He had several pieces on display, including an attractive pair of natural pearl earrings set with unheated Burmese rubies and unoiled emeralds (figure 23).

Vock discussed the global market for natural nacreous pearls, noting that it was greatly diminished by the 1980s due to the prevalence of cultured pearls. However, regions such as many of the Gulf countries and India did not feel pressure from the cultured pearl market. These countries have led a resurgence of natural pearl's popularity, specifically with Basra pearls. These originate in the Arabian (Persian) Gulf, and their namesake is the city of Basra in Iraq. Historically, Basra was the center of natural pearl commerce, with the greatest selection of natural pearls and the most informed dealers.

Vock mentioned that the most prized natural nacreous pearls today are from either the Gulf region or Australia. Currently, both regions produce what dealers describe as "new material," which are freshly harvested natural pearls. Natural pearls form in the mantle of the pearl mollusk shells, whereas cultured saltwater pearls grow inside the gonad of the mollusks. Many natural pearls have a large flat surface, similar to a button shape, because they grow against the mantle. For that reason, round, oval, and drop-shaped pearls are rarest and most valuable.

Figure 23. A pair of earrings with unoiled emeralds weighing about 8 ct total, natural pearls measuring 9.5–10.0 mm, unheated Burmese rubies weighing just under 5 ct total, and diamonds set in yellow gold. Photo courtesy of ProVockative Gems Inc.

*Figure 24. Left: The mother shell (*Mercenaria mercenaria*) and an 18K gold ring featuring a 14.43 × 14.63 mm lilac quahog pearl. Right: A rare collection of round quahog pearls ranging from 5.65 to 12.33 mm in diameter and in colors from white and beige to deep purple and tan. Photos by Robert Weldon; courtesy of ECIJA.*

When comparing pearls from the two regions, Vock explained, there are some differences. Basra pearls usually have a warmer bodycolor, while Australian pearls tend to be whiter. Also, Basra pearls are often rounder than their Australian counterparts. In fact, the Gulf region has the highest percentage of round natural nacreous pearls of any producing area. He credited this to the smaller shell of the Gulf region mollusks.

To see Alex Vock explain these common appearances with examples from his current collection, go to www.gia.edu/gems-gemology/spring-2023-gemnews-natural-nacreous-pearls.

Lisa Kennedy and Artitaya Homkrajae

Exceptionally rare pearls from ECIJA. At the GJX show, ECIJA (Santa Barbara, California) displayed a variety of natural, wild, nacreous, and non-nacreous pearls, including conch, oyster, scallop, abalone, and quahog pearls. Only 0.2% of all pearls in the current market are natural (S. Karampelas et al., "Raman spectroscopy of natural and cultured pearls and pearl producing mollusc shells," *Journal of Raman Spectroscopy*, Vol. 51, No. 9, 2019, pp. 1813–1821), and the authors found the non-nacreous collection especially notable.

ECIJA owner Aylene Norris and her husband, Jeremy Norris (Oasis Pearl), have been sourcing for 34 years and specialize in natural pearls. For the first time in Tucson, ECIJA displayed a collection of round quahog pearls (figure 24). Quahog pearls are produced in the bivalve mollusk *Mercenaria mercenaria* (figure 24, left), a type of saltwater clam native to the Atlantic Ocean. These non-nacreous pearls consist mainly of fibrous aragonite and organic matter. They are often not perfectly spherical but form irregular shapes such as button or baroque, making this set of round quahog pearls extremely rare (figure 24, right). Moreover, they exhibited an attractive and strong porcelaneous surface with sizes ranging from 5.65 to 12.33 mm in diameter. Quahog pearls are known for their unique range of colors, including white, beige, pink, lavender, purple, brown, and black. These 21 quahog pearls showed a wide color range, from white and beige to deep purple and tan (figure 24, right). According to Jeremy, lilac and deep purple are the most desirable and command the highest price. The color of a quahog pearl is determined by various factors, including the clam species and environmental and geochemical conditions.

Another rarity on display was a large (16.44 ct, 14.50 × 14.36 × 11.95 mm) deep purple, button-shaped non-nacreous pearl showing an obvious flame structure at its surface (figure 25). This pearl formed from one of the many *Spondylus* species, also known as "thorny" or "spiny" oysters, which are harvested on the western coast of the Americas as *Spondylus princeps* and *Spondylus calcifer/limbatus*.

Figure 25. This non-nacreous pearl weighing 16.44 ct and measuring 14.50 × 14.36 × 11.95 mm is reportedly from a Spondylus calcifer/limbatus *mollusk from the Sea of Cortez in Baja California. Photo by Robert Weldon; courtesy of ECIJA.*

Reportedly from *calcifer/limbatus* from the Sea of Cortez in Baja California, the pearl's large size, attractive purple color, and strong flame structure set its value. Previously, GIA has reported that flame structure is usually caused by subsurface to surface-reaching acicular inclusions (Fall 2016 Lab Notes, pp 303–304). Although several *Spondylus* pearls have been reported in *G&G* (Summer 2016 Micro-World, pp. 202–203; Fall 2016 Lab Notes, pp. 303–304), this is one of the largest and finest examples.

ECIJA also featured other nacreous and non-nacreous pearls for designers and buyers, including conch, scallop, and abalone pearls. Each of these species exhibits unique shapes and colors. Conch pearls are typically oval in shape and exhibit white, beige, brown, yellow, orange, pink, and red colors. They range in size from 1 mm to over 20 mm. Scallop pearls from *Nodipecten nodosus*, also known as "Lion's Paw" or "Mano de Leon," form button, oval, and baroque shapes that range from white and brown to rare purple or maroon colors. These exhibit beautiful reflective mosaic-like patterns on their surface. Abalone typically produce conical or baroque-shaped pearls exhibiting a combination of vibrant colors and a mirror-like luster. Symmetrical abalone pearls, especially in large sizes, are very rare.

While GIA has developed seven value factors to evaluate the quality of nacreous pearls (size, shape, color, luster, surface, nacre, and matching; see J.W.Y. Ho and S.C. Shih, "Pearl classification: The GIA 7 Pearl Value Factors," Summer 2021 *G&G*, pp. 135–137 and accompanying wall chart), it is difficult to set the value for non-nacreous pearls due to their rarity and individual characteristics. In addition, demand dictates the value and price of rare pearls. An increasing demand for conch pearls has attracted buyers from all around the world. Jeremy indicated that conch pearls are especially popular in the European, U.S., and Asian markets. Deep pink to red pearls exhibiting a strong flame pattern are the most desirable and have doubled in value over the last 10 years, whereas pastel colors continue to be a more affordable solution for designers and collectors alike.

Si Athena Chen

Chunhui Zhou
GIA, New York

New find of petroleum-included quartz from Madagascar. At the Tucson Gem and Mineral Show (TGMS), a new find of quartz with petroleum inclusions was offered for sale by Hidden Gem Gallery (Portland, Oregon). According to owner G. Moses Samora, the material is from the Andranotokana Massif in the Alaotra-Mangoro region of eastern Madagascar. Petroleum inclusions in quartz have been seen for a number of years from many deposits, most notably from Baluchistan, Pakistan (Spring 2004 Gem News International, pp. 79–80). The petroleum in these quartz crystals from Madagascar appeared brownish yellow and, as with many other petroleum inclusions in quartz, reacted to long-wave UV light with yellow to blue fluorescence (figure 26).

Microscopic examination revealed numerous complex fluid inclusions containing obvious brownish yellow petroleum, a gas bubble presumed to be methane, dark solids of what was likely asphaltite, and a colorless immiscible liquid that was probably water (figure 27). Interestingly, in some fluid inclusions the methane bubble was mobile provided there was enough available space within the petroleum-filled cavities. These components are consistent with petroleum fluid inclusions in quartz from other deposits. When exposed to long-wave UV light, the petroleum component strongly fluoresced light yellow (which appeared blue in the photomicrographs), as has been previously observed in similar material. The two crystals from this new deposit displayed a scepter morphology, which seems unusual, though it remains unclear whether this is diagnostic for the locality or just unique to these specific examples.

Figure 26. These two quartz crystal scepters containing a multitude of complex petroleum fluid inclusions (left) that fluoresce yellow to blue to long-wave UV light (right) are from a new deposit in Madagascar. The larger crystal weighs 11.05 ct and measures 22.81 mm in length. Photos by Annie Haynes; courtesy of Hidden Gem Gallery.

Figure 27. The new find of quartz from Madagascar contained complex fluid inclusions consisting primarily of petroleum, methane, asphaltite, and water (left). When exposed to long-wave UV light, the petroleum appeared to fluoresce a strong yellow. However, the digital camera used to capture the image registered the fluorescence as a blue color (right). Photomicrographs by Nathan Renfro; field of view 2.81 mm.

Microscopic inclusions in quartz are enjoyable to examine, and petroleum inclusions are of particular interest to the collector due to their spectacular UV reaction. The introduction of this new quartz find at the Tucson show is an exciting addition to the gem and mineral trade.

Nathan Renfro and John I. Koivula
GIA, Carlsbad

Bright orange sapphire from Greenland. The Aappaluttoq mine in Greenland is home to the oldest known ruby-bearing rocks on Earth. These host rocks are nearly three billion years old (A. Polat et al., "New age (ca. 2970 Ma), mantle source composition and geodynamic constraints on the Archean Fiskenæsset anorthosite complex, SW Greenland," *Chemical Geology*, Vol. 277, No. 1-2, 2010, pp. 1–20). This deposit was initially known for producing translucent to opaque ruby and pink sapphire, much of it cut into cabochon form. However, transparent material has always been found in this mine and makes up about 5–10% of the production.

At the AGTA show, Greenland Ruby displayed many examples of attractive transparent ruby and pink to orangy pink sapphire, including several fancy-color sapphires in sizes greater than one carat (figure 28; see also pp. 145–149 of this issue). These fancy colors are achieved by heat treating nearly colorless to slightly pink transparent material. A transparent bright orange sapphire weighing 0.89 ct and measuring 6.41 × 5.02 mm (figure 29) immediately caught our eye. Martin Viala, product manager for Greenland Ruby, shared with us a video of the original 1.07 g sapphire rough (visit www.gia.edu/gems-gemology/spring-2023-gemnews-bright-orange-sapphire-greenland). This unusual stone was mined in late 2019 and heated in May 2022. Viala noted that it was a textbook example of a chromium trapped-hole ($h^{\bullet}$–Cr^{3+}) chromophore (E.V. Dubinsky et al.,

Figure 28. A 1.28 ct heated pink round brilliant sapphire. Photo by Robert Weldon; courtesy of Greenland Ruby.

Figure 29. A 0.89 ct heated orange oval brilliant sapphire. Photo by Robert Weldon; courtesy of Greenland Ruby.

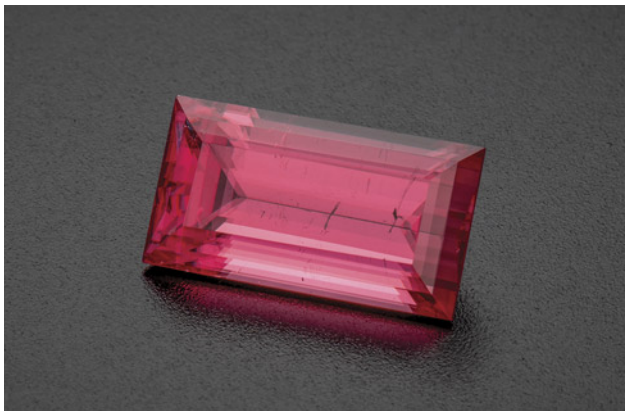

Figure 30. A 7.94 ct rectangular step-cut rhodochrosite from the Sweet Home mine in Colorado's Alma Mining District. Photo by Robert Weldon; courtesy of Barker & Co.

"A quantitative description of the causes of color in corundum," Spring 2020 *G&G*, pp. 2–28).

Jennifer Stone-Sundberg and Si Athena Chen

Sweet Home mine rhodochrosite from 1888. At AGTA, Ann Barker and Tori Lopez of Barker & Co. (Scottsdale, Arizona) exhibited a 7.94 ct rectangular step-cut rhodochrosite (figure 30) with a provenance dating back more than a hundred years. The stone is from the Sweet Home mine in Colorado's Alma Mining District, at an elevation of about 3,300 m in the Rocky Mountains.

Sweet Home was established as a silver mine in 1872. Miners initially discarded most of the rhodochrosite found in association with the silver ore because it interfered with the amalgamation process used then in silver mining. But the large, highly saturated, and nearly perfectly formed crystals later discovered there are some of the world's finest rhodochrosite specimens.

Rhodochrosite was first described in the mineralogical literature in 1813 based on specimens from what is now Romania. In 1887, George F. Kunz wrote of gem-quality rhodochrosite in Colorado, noting it was the first source with such large and transparent crystals. Most of the rhodochrosite available worldwide was light pink, opaque, and often banded—typically used for beads, cabochons, and carvings. This source introduced pink to red gem-quality single-crystal rhodochrosite, which is rare. The gemstone became more widely known in the late 1930s, after a German gemologist found large volumes in Argentina's Catamarca Province high in the Andes. (In Argentina, the use of rhodochrosite dates back to the ancient Incas, who are said to have believed it was the solidified blood of their fallen rulers.)

The step-cut stone's traceable history began in 1888, when a shaft collapse resulted in a 32.61 ct cleavage fragment. Miner Edward Abbott kept it and in 1925 gave it to Denver businessman Edwin Spray, who later owned the mine. The same year, Sweet Home miners found large specimens on quartz matrix, many of which were sold to museums in the U.S. and Europe. In 1968, the fragment made its way from Spray's widow, Eleanor, through a friend of the family to geologist and mineral collector Charles Trantham in California. In 1981, Glenn Vargas, a gem and mineral dealer and university instructor, expertly cut the stone. Rhodochrosite often presents challenges for cutting due to its low hardness (3.5–4.0 on the Mohs scale) and perfect rhombohedral cleavage.

Rhodochrosite mining at Sweet Home expanded significantly in 1991—long after silver production ended in the 1960s—when Eleanor Spray's nephew, F. Leonard Beach, leased the property to a group of investors led by Collector's Edge Minerals. The group found several new pockets and in 1992 uncovered the Alma King, a 14.2 × 16.5 cm deep cherry red rhombohedron, the world's largest known fine rhodochrosite crystal.

The Sweet Home mine closed in 2004, but the group went on to develop the associated Detroit City mine, which has produced some fine specimens since 2019.

Erin Hogarth

New tourmaline pockets in San Diego County's Pala District. At the AGTA show, Bill and Carl Larson (Pala International, Fallbrook, California) shared details about new pockets uncovered at the Tourmaline King mine. The first was discovered in January 2022—the first major find at the mine in more than a hundred years, and the first in Southern California since the "Big Kahuna" pocket at the Oceanview mine in 2010. "We've hit off and on three or four pockets, some of which are very good," Bill said.

The Larsons showed us several stones, including a 16.96 ct emerald-cut green tourmaline (figure 31) from rough found near the first pocket in 2022. Bill said the green tourmaline is relatively uncommon for the Pala District. "The green has actually been transparent enough to

Figure 31. A 16.96 ct emerald-cut green tourmaline from rough found near a new pocket at the Tourmaline King mine. Photo by Robert Weldon; courtesy of Pala International.

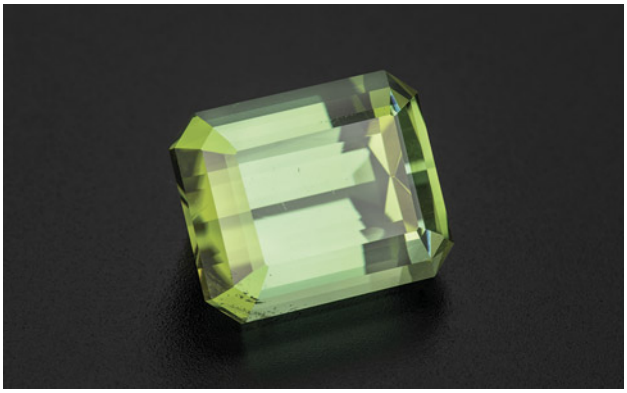

Figure 32. Rubellite tourmaline rough (440 g) from one of the Tourmaline King mine's new pockets. Photo by Robert Weldon; courtesy of Pala International.

facet," Carl added. "That's been the best material so far." The new pockets have also produced about 3 kg of fine-color rubellite rough (figure 32).

The Tourmaline King mine's main tunnel produced eight tons during San Diego County's massive output of tourmaline in the early nineteenth century, which also involved the Pala District's Tourmaline Queen, Pala Chief, and Stewart mines, as well as Mesa Grande's Himalaya mine. (There was a resurgence of mining at Pala in the 1970s.)

Around 1920, mine owner R.M. Wilke and his crew installed a new tunnel below the main one. "They hit this very dangerous zone right before they hit the pegmatite," Bill said. Here they encountered a shear zone that caused a roof collapse. Wilke abandoned mining efforts around 1922.

Pala International's mining partner, San Diego Mining Company, reclaimed the tunnel several years ago and began extending it in 2019. "They got to the dangerous area, and then they backed up about 10 meters and went around and hit the pegmatite," Bill said. "Now they're in from the front to the back, where we're hitting tourmaline."

Carl recalled his initial look at the first new pocket. "Kiel Snyder stopped me and said, 'Everyone else gave up here,'" he said. "He just believed in it and kept going. Then they hit a small pocket—nothing of note, but something that said, 'There are stones here.' I think they called that the 'Never Give Up' pocket. Within 10, 15 feet, they hit that first pocket."

The crystals were large and well formed, and the miners uncovered a very large terminated quartz crystal, a collector specimen. Carl said the crystals in this pocket lack the rubellite color and are not typical of the mine, making them inadequate for cutting and cabbing. But in January of 2023, they discovered a pocket of beautifully colored red rubellite, too included for faceting but suitable for cabbing and carving. "We're hoping that we'll hit some more gemmy transparent material," he said.

"It's really exciting to have an active mine in Southern California because of its rich history," Carl said. "At the turn of the century we were hitting a lot, and then it was vacant for so long. So to have some energy coming in with new material is exciting."

Erin Hogarth

Vibrant green grossular garnet "Transvaal jade." At the Pueblo show, Tom Schneider of TMS Gems (San Diego, California) offered "Transvaal jade" rough displaying an exceptionally vivid green color. Also known as "African jade" or "South African jade," this is not a true jade (jadeite or nephrite). The stone is instead a grossular garnet whose trade name is derived from its massive habit and green color, and the type locality. Specimens of this material are typically more translucent and lighter in color (J. Frankel, "Uvarovite garnet and South African jade (hydrogrossular) from the Bushveld Complex, Transvaal," *American Mineralogist*, Vol. 44, No. 5-6, 1959, pp. 565–591). Nested in a fine-grained chromite matrix, the opaque green portion of the stone in figure 33 had a refractive index of 1.731 and was inert to both long-wave and short-wave ultraviolet radiation.

The sample was identified as grossular garnet using Raman spectroscopy and further classified as a grossular-andradite garnet using X-ray fluorescence chemical analysis and the naming convention proposed in 1995 (M.L. Johnson et al., "Gem-quality grossular-andradite: A new garnet from Mali," Fall 1995 *G&G*, pp. 152–166). The chemical

Figure 33. This 110.4 g partially polished rough grossular garnet "Transvaal jade" and three polished cabochons (41.95–92.87 ct) display unusually vibrant green colors between seams of dark chromite matrix. Photo by Diego Sanchez; courtesy of TMS Gems.

Figure 34. Alex Skachkov of Misfit Diamonds. Photo by Jennifer Stone-Sundberg.

data show 80.83 mol.% grossular ($Ca_3Al_2Si_3O_{12}$), 10.50 mol.% uvarovite ($Ca_3Cr_2Si_3O_{12}$), 7.11 mol.% andradite ($Ca_3Fe_2Si_3O_{12}$), and trace amounts of other garnet. Garnets in the grossular to andradite range can show 4.64–20.91 wt.% Fe_2O_3 (Johnson et al., 1995) and typically have low chromium values (≤0.23 wt.% Cr_2O_3) (C.M. Stockton and D.V. Manson, "A proposed new classification for gem-quality garnets," Winter 1985 *G&G*, pp. 205–218). Increased iron content will impart a yellow, orange, or brown color component, while the most intensely green stones owe their color to chromium and possibly vanadium (Johnson et al., 1995). The low iron content (2.49 wt.% Fe_2O_3) and elevated chromium content (3.50 wt.% Cr_2O_3) of this sample likely resulted in its remarkable coloration.

The chromium-rich nature of this particular specimen produced a beautiful vibrant green with a high-polish luster, making it an outstanding example of this material.

Kendra Carty and Amy Cooper
GIA, Carlsbad

DIAMONDS

Misfit Diamonds: Beauty in the imperfect. At the AGTA show, we spoke with Alex Skachkov of Misfit Diamonds (Vancouver, Canada) about some of their unusual diamonds (figure 34). When asked what was popular, he showed us their aptly named "salt and pepper" diamonds (see also figure 5 of the Tucson 2023 overview), which contained eye-visible black and white inclusions. These had a very distinct look and were cut into various nonstandard shapes (figure 35).

Skachkov described the appeal of these unique and beautiful "imperfect" diamonds, particularly to younger

Figure 35. "Salt and pepper" diamonds. Left to right: a 4.30 ct hexagonal step cut, a 5.56 ct octagonal step cut, a 3.58 natural-color orange cushion cut, and a 3.39 ct pear cut. Photo by Robert Weldon; courtesy of Misfit Diamonds.

designers and consumers. In his words, younger customers are not necessarily interested in absolutely flawless gems. Rather, many are looking for gems that charm in their distinctive and rare "perfect imperfection." He noted that these diamonds are also a more budget-friendly option. In addition to the "salt and pepper" diamonds, we got a close look at diamonds and sapphires cut into nontraditional shapes, including slices (figure 36).

Skachkov mentioned that many of their customers now look for full disclosure of the entire mine-to-market custody chain. Misfit Diamonds provides this information whenever possible, though at times their diamonds arrive in mixed-origin parcels, with stones from a variety of global locations. Moving forward, they aim to meet the challenge of reporting full chain of custody, as they predict increasing demand for this feature.

Jennifer Stone-Sundberg and Si Athena Chen

Figure 36. Nontraditional diamond cuts and slices in a range of sizes. Photo by Jennifer Stone-Sundberg; courtesy of Misfit Diamonds.

Figure 37. The "Seven Sisters" ring in 18K gold with 17 bezel-set diamonds (0.55 carats total) and 22 sapphires ranging in size from 2.5 to 4.0 mm in blue, orange, mandarin, pink, and green (3.15 carats total). Photo by Robert Weldon; courtesy of Sean Hill Designs.

JEWELRY DESIGN

Sean Hill: Exquisite jewelry designs. At the GJX show, Sean Hill of Tucson presented some striking jewelry designs with masterful control of shape and line. A gold ring set with diamond, blue sapphire, and fancy-color sapphire (figure 37) drew us into his booth. Dr. Hill, a self-taught jeweler, has been active designing and handcrafting jewelry since 1998, after a previous career as a university professor in literature and philosophy. His academic and philosophical nature is immediately evident when discussing design, and his meticulous attention to space and volume becomes more apparent the longer one studies his pieces. The "Seven Sisters" ring in figure 37 raises each stone to a unique height above the flat base, filling the rectangle with an appealing placement of 17 colorless diamonds interspersed among 22 sapphires.

A stunning pair of 18K white gold earrings featuring both diamond slices and faceted diamonds (figure 38) is a case study in filling a plain geometric shape to bring it to life. As Dr. Hill said in describing the piece, "A rectangle is a basic shape, a self-imposed constraint. It is how you choose to fill it that makes it interesting." Adding to the design quality, the rectangles are not actually flat but gently curved so that the earrings fit seamlessly on the ear.

A pair of 18K gold earrings with brilliant-cut diamonds and sapphires (figure 39) illustrates a modern and considered take on the classic chandelier earring, with squares and rectangles outlining floating round gems on delicate strings of gold. Dr. Hill explained some of his jewelry philosophy: "You can always take a stone for its beauty, color, and cut, set it into a finding, and it is all about the stone. But how do you make it into art?"

Jennifer Stone-Sundberg and Si Athena Chen

Figure 38. "Rose Cut" 18K white gold and diamond earrings. The faceted diamonds are 1.5–2.0 mm in diameter. Photo by Robert Weldon; courtesy of Sean Hill Designs.

Figure 39. "Event Horizon" earrings in 18K gold, diamond (0.07 carats total), and orange, mandarin, pink, green, and blue sapphire (5.2 carats total). Photo by Robert Weldon; courtesy of Sean Hill Designs.

Figure 40. These handcrafted jewelry pens are created with silver, embellished with 24K gold, and inlaid with diamond, sapphire, and crushed emerald. Left: The peacock design is a miniature painting coated in clear enamel. Right: A pen with fine metal engraving and dimming just below the 24K gold nib. Photo by Robert Weldon; courtesy of Zeki Karaca.

Zeki Karaca Jewelry: Luxury pens. Some of the most original work we saw at the GJX show included bejeweled pens made by Turkish designer Zeki Karaca (figure 40). These intricate pens feature exquisite details and fine craftsmanship in metalworking, enameling, engraving, inlay, and stone setting. In addition to pens, Karaca also creates other desk items such as letter openers and magnifying glasses (figure 41).

Born in Istanbul, Karaca has 41 years of jewelry-making experience, originally designing jewelry to sell in the Grand Bazaar. To apply his experience and creativity to different designs and styles, he began making luxury pens and products three years ago. He first ventured into these new products by crafting silver gemstone handles for Damascus steel knives. After finding success there, he expanded to meet the demand for luxury pens, letter openers, and magnifying glasses.

Figure 41. Silver magnifying glass with 24K gold embellishments, inlay, carvings, and diamonds. Photo by Robert Weldon; courtesy of Zeki Karaca.

Each pen takes about six months to design and craft. All production steps are done by hand, making each item one of a kind. After designing an item, Karaca creates a silver body using fold forming, with the folds created using emery sheets. Engraving is executed by a master engraver using different nibbed steel pens, and dimming is used to emphasize the engraving. Karaka incorporates diamond, sapphire, emerald, and ruby into the designs and uses 24K gold for design highlights. Miniature paintings, such as the peacock on the pen cap in figure 40 (left), are created by hand with a small brush and then coated with a transparent enamel for protection. For micro-mosaics, gemstones such as emerald are crushed and added to the pen body, as seen in both pens in figure 40. The pen parts are welded together with a laser, and then the 24K gold nibs are added.

With high demand for his products from collectors, Karaca continues to explore additional high-end objects as well as custom designs for some clients.

Jennifer Stone-Sundberg and Mimi Travis
GIA, Carlsbad

Brenda Smith Jewelry designs. Brenda Smith Jewelry has earned four AGTA Spectrum Awards to date for design excellence. At this year's AGTA designer showroom, Smith presented three masterpieces to the authors: two award-winning rings featuring pearl and blackened gold lace and an opulent pair of earrings featuring *millefiori* faces.

Smith's most prized creation is her Lace Ring design. She shared her white Lace Ring featuring a large cultured pearl accented with gold lace, sapphires, and diamonds (figure 42A), followed by a black Tahitian pearl Lace Ring with

Figure 42. A: This Lace Ring is crafted in 18K rose gold with blackened gold lace, featuring a cultured freshwater pearl measuring 16.5 mm in diameter, enclosed by natural-color pink and lavender sapphire round brilliants weighing 2.86 carats total. The shank of the ring is embellished with 0.06 carats of diamonds. B: This Tahitian pearl Lace Ring is created in 18K white gold with sandblasted and blackened gold lace. The cultured Tahitian pearl measures 16.0 mm and is surrounded by round brilliant diamonds, 1.35 carats total. The rubies in the shank weigh a total of 0.08 carats. C: A handmade doily crocheted by Smith's grandmother. Photos courtesy of Brenda Smith.

blackened gold lace, rubies, and diamonds (figure 42B). Inspired by her grandmother's handmade crocheted doily featuring a pineapple motif (figure 42C), the rings were created as a tribute to her memory. In 2021, the white freshwater pearl ring won Best Use of Pearls in the AGTA Spectrum competition and the Tahitian pearl ring won the InDesign Award in the category of Pearl Jewelry Over $5,000.

Figure 43. These "Gibson Girl" millefiori *earrings in 18K white gold contain Paraíba tourmalines (1.11 carats total), pink tourmalines (1.54 carats total), and 0.56 carats of aquamarine. Photo courtesy of Brenda Smith.*

Smith's one-of-a-kind "Gibson Girl" earrings (figure 43) are inspired by the Austrian symbolist painter Gustav Klimt. Klimt's paintings combined realistic faces with geometric clothing, and Smith mirrored this style to create this high-end piece of jewelry. The technique used to create the girl faces is *millefiori*, which means "thousand flowers" in Italian and produces slices from canes with concentric and colorful patterns. *Millefiori* techniques can be used to make jewelry, decorative objects, candy, and art pieces. Creating these objects requires a skilled artisan who possesses a deep understanding of material properties, considerable experience, and patience. American artist Barbara McGuire handcrafted the complex face canes for the earrings by arranging and embellishing polymer clays to create a lifelike image. Though *millefiori* objects are commonly used in decorative pieces, Smith's design incorporates a harmonious blend of colored gemstones expertly paired and crafted to create a lively figure with a unique personality and color scheme, making it an extravagant and elegant piece of jewelry.

Si Athena Chen and Jennifer Stone-Sundberg

YNY Jewels: Designer Surbhi Pandya. A dazzling pair of carved tanzanite earrings (figure 44) caught our attention at the GJX show. Designer Surbhi Pandya of YNY Jewels (New York), who goes by the single name Surbhi, described the significance of the carving featured on each of the large unheated tanzanite crystals. Depicted in violet and green is the lotus blossom, a flower with ancient cultural significance in India, rising with its deep roots from the mud without stains, symbolizing purity and strength. As the blossoms close up at night and reopen the next day, they also symbolize rebirth. Each carving is immediately surrounded by a ring of blue Kashmir sapphires and emeralds, followed by colorless diamonds and bright green tsavorite garnets. Each

Figure 44. Surbhi's "Orient" earrings with tanzanite carvings surrounded by blue sapphires, emeralds, white diamonds, and tsavorite garnets with an upper flower-shaped dangle composed of faceted tanzanites, emeralds, and pink sapphires, all set in 18K white gold. The total diamond weight for the pair is 1.60 carats, and the total colored stone weight is 62.23 carats, 48.32 carats of which are from the two tanzanite carvings. Photo by Robert Weldon; courtesy of YNY Jewels Inc. and Karats Inc.

upper dangle contains faceted slices of tanzanite and emerald with a central hot pink sapphire. She also shared a pendant with a paisley-shaped unheated tanzanite similarly containing a lotus carving (figure 45). She explained that the paisley shape represents continuity and life.

Figure 45. An 18K white gold pendant containing a paisley-shaped unheated tanzanite with a lotus blossom carving, surrounded by pavé-set black diamonds and pink and purple princess-cut Sri Lankan sapphires. The total weight of the diamonds is 1.00 carats, and the colored stones total 23.40 carats. Photo by Robert Weldon; courtesy of YNY Jewels Inc.

Figure 46. Designer Surbhi. Photo by Jennifer Stone-Sundberg.

Surbhi (figure 46) has been making jewelry for 20 years and was trained by her father, Yogendra Sethi, a renowned artist in India. She described designing jewelry as a journey filled with energy. She does not make jewelry to please herself, but out of a drive to create things that speak to others. Surbhi shared stories of customers' deeply personal connections with her jewelry, a profoundly rewarding experience for her as an artist.

Jennifer Stone-Sundberg and Si Athena Chen

RESPONSIBLE PRACTICES

Ethical supply chain practices in Africa with Virtu Gem. This year marked Tucson's fourth Ethical Gem Fair, a market cooperative of ten responsibly sourced gemstone suppliers (see Spring 2020 GNI, pp. 177–179). The fair was held January 28–31 at the Scottish Rite Cathedral. Virtu Gem sells gemstones directly from artisanal mining communities in Kenya, Malawi, and Zambia (figure 47) and debuted at the fair in 2022. We spoke with cofounder Susan Wheeler and Percy Maleta, Virtu Gem's country exporter and ambassador in Malawi, about its beginnings, programs, and impacts.

Wheeler said more new customers come to the Ethical Gem Fair each year. "All the large companies come by, too," she said. "There were a lot this year that everybody was surprised by. I think that the awareness of what artisanal mining is and what it can be is spreading."

Figure 47. Some of Virtu Gem's larger gemstones from Kenya, Malawi, and Zambia at the Ethical Gem Fair. Clockwise from top: 45.00 ct citrine, 32.33 ct rutilated quartz, 9.80 ct aquamarine, 21.65 ct citrine, 9.99 ct aquamarine, 12.32 ct aquamarine, 17.20 ct aquamarine, and 20.15 ct citrine (center). Photo by Robert Weldon; courtesy of Virtu Gem.

Virtu Gem gives artisanal miners, cutters, and traders formal access to international markets and began as a project of Wheeler's nonprofit Responsible Jewelry Transformative (RJT). Virtu Gem's programs also offer training in cutting and basic gemology and help miners improve safety, labor, and environmental conditions at the mines, all with a focus on women. Their gemstone prices include a 10% premium that goes toward fulfilling the mining communities' various needs. During the height of the COVID-19 pandemic, the premium was used for food drives in all three countries and personal protective equipment for Kenyan women miners; currently it goes to the purchase of safety equipment (figure 48).

Wheeler and cofounders Jessica Hudson and Monica Gichuhi (figure 49) began selling gemstones from Zambia online in 2020, after the pandemic forced the cancellation of a conference they had planned there that would have provided a market for traders. "There was a call to action from the Organisation for Economic and Co-operative Development (OECD) to support all the artisanal miners because no one was coming to the country to buy their stones," Wheeler said. The OECD's Call to Action for Responsible Mineral Supply Chains cited COVID-19's disproportionate impact on artisanal and small-scale miners, who make up more than 80% of the global mining workforce and already face inequities in the supply chain. Wheeler and Hudson are both jewelry designers; Gichuhi is a founding member of the Association for Women in Extractives in Kenya (AWEIK). Her connections with mining associations in Zambia were a starting point.

Beginning in 2021, Virtu Gem received two grants through RJT from the World Bank's Extractives Global Programmatic Support fund. The fund's purpose is to promote sustainable and inclusive mining in developing countries and thereby reduce poverty. The grants allowed them to expand into Kenya and Malawi, hold virtual cutting workshops, and implement CRAFT Code in eight mines. ("CRAFT" stands for Code of Risk mitigation for Artisanal and small-scale miners engaging in Formal Trade.) Virtu Gem also hired experienced international consultants.

Figure 48. Artisanal emerald miners in Zambia celebrate a donation by Virtu Gem of safety equipment and a jackhammer. Photo courtesy of Virtu Gem.

Figure 49. Left: Virtu Gem cofounders Jessica Hudson, Monica Gichuhi, and Susan Wheeler on a recent visit to Malawi. Right: Percy Maleta, the organization's country exporter and ambassador in Malawi, examines a rough gemstone. Photos courtesy of Virtu Gem.

"There's been a huge amount of progress over the past two years," Wheeler said. The funding helped Virtu Gem develop a strong foundation, she said, and grow enough to be able to pass any chain of custody standard for large-capacity buyers.

While Virtu Gem has had success in all three countries, Wheeler said Kenya has seen the most because some in the trade already had Ultra Tec cutting machines and were selling to the international market. "After the first few purchases we did, word spread," she said. "People were showing up with 50 gems at a time to process." Miners can also bring gems to the country coordinators for cutting.

Virtu Gem's gemstones are cut in each country and tracked with Provenance Proof Blockchain. They include amethyst, aquamarine, citrine, moonstone, rhodolite and other garnets, in all three countries; emeralds in Zambia; tsavorite in Kenya (figure 50); and color-change garnet in Malawi. The three countries also produce tourmaline in various colors, including pinkish orange ("sunset") in Malawi and Zambia and golden in Kenya and Malawi. Production of morganite from newly discovered deposits in northern Malawi recently began.

Virtu Gem has helped miners implement CRAFT Code at four mines in Zambia, two in Malawi, and two in Kenya. CRAFT Code is designed to improve safety, labor, and pay conditions through education at the mines. Its components include mine site certification, safety standards and equipment, and environmental planning, including carbon data tracking and reduction.

CRAFT Code has an emphasis on protecting women, and Wheeler said they focused on women for the associated training. Focusing on woman-owned mines was more difficult, however. "It's a big challenge for women to own any land at all, especially in Zambia, Kenya, and Malawi," Maleta said. In Zambia, two of the mines—one emerald and one amethyst—were woman-owned, and in Kenya they worked with a young woman whose family owned a mine.

One of Virtu Gem's benefits is helping artisanal miners formalize their mining process. In Malawi, country coordinator Chiko Manda wanted to focus on rhodolite. Maleta said women account for roughly 80% of rhodolite production there (figure 51). Rhodolite is alluvial and best mined

Figure 50. Rough tsavorite mined from a site in Kenya. Photo courtesy of Virtu Gem.

Figure 51. Artisanal rhodolite miners in Malawi. Photo courtesy of Virtu Gem.

during the rainy season in Malawi, when the women are busy tending their gardens. Virtu Gem worked with a young couple, Ben and Tamara, who did not have a mining certificate.

"The chief of the Chewa people didn't want the women mining," Wheeler recalled. "Ben had to go and prove himself to the chief, that he wasn't going to take advantage, and that the women could still do their agriculture." Ben joined Virtu Gem's calls with miners in Kenya and Zambia who shared advice. "He ended up getting permission to mine on the land and the blessing of the chief," she said. "He sent me on WhatsApp a picture that he had gotten his certificate. He was so happy." Maleta said that Ben recently received another land permit and is applying for a second mining certificate. "That was a way we could still work with the women," Wheeler said.

Wheeler mentioned the danger of holding a large amount of gemstones in an informal market, which Ben and Tamara encountered with a quantity of rhodolite. "You have the paradox of the women's safety," she said. "Everybody hears about it, and you get all these other dealers and traders coming in. How are they going to get a fair price? Yet they can't hold on to it." She said Ben called his friends and pleaded with them to purchase some of the rhodolite. She would like to see a formal system to address this type of scenario.

Maleta said the past four or five years have seen an influx of Kenyans and Zambians to Malawi to buy gems, some of whom export them back home and misrepresent the source country. By exporting directly from Malawi, Virtu Gem has improved supply chain transparency.

Maleta said Virtu Gem pays more than the informal market, but convincing people to participate can be a challenge. "To have someone leave a stone with you and wait—for maybe two months, three months—it hasn't been easy," he said. "But we have people who understand the process, who know that the stone they are leaving with Virtu will be sold, but also understand that if it's not sold, it will be returned. That is trust."

"I was surprised by the lack of trust at the beginning," Wheeler said. "We have to work hard to earn the trust from everybody in the gemstone community. We couldn't have done this without our partner, Monica Gichuhi, working within the communities, and our country coordinators." She mentioned Caroline Muchira in Kenya, who is also a cutter and a GIA Graduate Gemologist; Manda in Malawi; and Pauline Mundia in Zambia, a respected woman leader whom everyone calls "Mama Pauline."

"Living up to expectations is hard every single day," Wheeler said. "Tucson is hard because we don't own anything on display. Those are people sending us their stones that they've invested in. Before, they would have just sold them and not invested in separating parcels and cutting. That's a lot of pressure. We've earned some of that trust, and we really have worked hard to earn that."

"It's a dream come true for many to have their stones sold at this level," Maleta said. "For us, for the country, for the people who are trading, the future is bright."

Erin Hogarth

SYNTHETICS AND SIMULANTS

Luminescent synthetic garnet-like crystals. At the 22nd Street show, the author spoke with Tim Challener of Turtle's Hoard (Raleigh, North Carolina), who was selling some unique rough and faceted luminescent synthetic garnet-like crystals, which he referred to as "lumogarnets." After 12 years in the gem business, Turtle's Hoard began selling only laboratory-made materials in March 2022. Challener noted

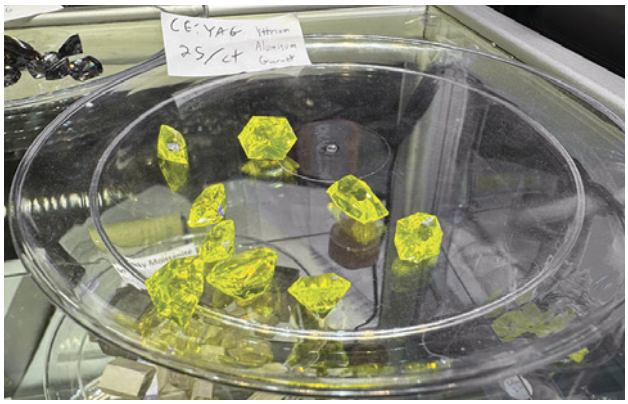

Figure 52. Yellow to greenish yellow faceted cerium-doped YAG "lumogarnets" ranging from 4 to 12 ct apiece. Photo by Lisa Kennedy; courtesy of Turtle's Hoard.

that their best-selling gemstone is Ce:LuAG, lutetium aluminum garnet ($Lu_3Al_5O_{12}$) doped with cerium. This material was introduced to the optics industry in the late 1990s and acts as a scintillator, a fluorescent crystal that absorbs high-energy radiation such as X-rays or gamma rays and reemits them as lower-energy visible light that is much easier to detect. LuAG is closely related to YAG electronically and both have the same garnet structure, yielding a gem with similarly excellent optical and gem properties (see figure 52).

Yttrium aluminum garnet, known as YAG ($Y_3Al_5O_{12}$), a lab-grown crystal that crystallizes in the cubic garnet structure, was one of the most popular diamond simulants from the 1960s to the mid-1970s due to its relatively good hardness (about 8.25 on the Mohs scale) and brilliance. Cartier's replica of the 69.42 ct Taylor-Burton diamond famously used YAG. Gadolinium gallium garnet, known as GGG ($Gd_3Ga_5O_{12}$), was the next garnet-like material to be used as a diamond simulant. GGG is slightly more brilliant and dispersive than YAG but scratches fairly easily due to its lower hardness (about 6.5 to 7.5 on the Mohs scale).

Most of these garnet-like crystals are doped with various rare earth elements such as neodymium, erbium, cerium, and ytterbium. These dopants not only increase the materials' value in the optics industry but also yield the variously colored synthetic garnet-like crystals seen in the gem and jewelry industry today.

These synthetic garnet-like crystals are most commonly produced by the Czochralski method, also known as the pulling method. In this melt process, the boule (a cylindrical synthetic crystal produced by a melt process) grows from a thin cylindrical seed crystal that is dipped into a melt of the desired garnet composition. The seed is rotated and then lifted very slowly at a controlled rate, allowing the melt to crystallize onto it. The material produced is extremely pure, with few inclusions or none at all. However, the material is not actually made for the gem and jewelry industry; rather, those in the industry can only purchase some of the less-perfect material and off-cuts of the boules to facet and sell (figure 53).

Challener explained, "They are lab-created, but each one has its own history beyond its use as a gem. And while there have been conflicting messages about whether some lab-grown stones, particularly lab-grown diamonds, are truly eco-friendly, the materials we work with are an inevitable byproduct of necessary crystal growth. Our modern lives rely on these materials being grown—we can't have cell phones without lithium niobate or modern PET scanners without scintillators—so there isn't really any additional waste associated with them."

Turtle's Hoard offered a variety of "lumogarnets," including rough and faceted luminescent yellow and yellowish green cerium-doped GAGG (gadolinium aluminum gallium garnet, $Gd_3Al_2Ga_3O_{12}$), cerium-doped LuAG, and cerium-doped YAG (see again figure 52). In addition, they displayed rough grayish purple neodymium-doped YAG, rough and cut greenish blue ytterbium-doped YAG (figure 54), rough pinkish orange erbium-doped YAG, and rough and faceted green chromium-doped YAG, a green stone with strong red fluo-

Figure 53. The top of a YAG boule doped with cerium and neodymium and produced by the Czochralski method, measuring approximately 36 mm in diameter and 45 mm tall. Parts of the boule that cannot be used for scientific purposes can be sold to the gem and jewelry trade for faceting. Photo by Lisa Kennedy; courtesy of Turtle's Hoard.

Figure 54. Greenish blue rough and cut ytterbium-doped YAG. The cabochon in front is 14 × 10 mm. Photo by Lisa Kennedy; courtesy of Turtle's Hoard.

rescence showing simultaneous flashes of green and red based on lighting, dubbed "Christmas garnet." Although synthetic and possessing a garnet-like structure, YAG, GGG, LuAG, and GAGG are not synthetic garnet, since they lack the chemistry of any garnets known in nature.

Lisa Kennedy

EXHIBITS

GIA Museum's "Paint the Town Ruby Red" exhibit at TGMS. At the Tucson Gem and Mineral Show, the GIA Museum exhibited a Burmese ruby and diamond necklace and earrings against a backdrop of the necklace fluorescing in ultraviolet light (figure 55). The necklace contains 39 untreated rubies from Mogok totaling 83.73 carats and 302 diamonds totaling 42.62 carats. The largest ruby is 5.00 ct.

The exhibit highlighted the "magic ingredient"—chromium—that gives ruby not only its color but also its fluorescence. Mogok rubies are renowned for their high concentration of chromium and low concentration of iron. The latter element, if present in a high enough concentration, quenches all or part of the red fluorescence produced by the chromium. This fluorescence is an important factor in the high value of Mogok rubies.

TGMS began in 1955 and is one of the longest-running gem and mineral shows in the world. GIA Museum curator Terri Ottaway said she was thrilled at the opportunity to showcase such a gorgeous necklace and include a bit of chemistry and geology for the gem and mineral enthusiasts.

Erin Hogarth

GIA Library wins exhibit award at TGMS. GIA's Richard T. Liddicoat Gemological Library and Information Center was awarded the Betty Clayton Gibson Memorial Trophy for Best Museum Exhibit for 2023 at the Tucson Gem and Mineral Show. The winning exhibit illustrated the importance of mercury-free gold mining (figure 56). Historically, mercury has been used in artisanal and small-scale gold mining because of its ability to bond with gold to form an amalgam, but its high toxicity and negative effects on humans and wildlife have led to increased emphasis on mercury-free options for mining gold.

The exhibit featured a traditional wooden bowl used for gold panning, along with many of the library's books on ecological jewelry and responsible and sustainable mining and jewelry practices.

"This exhibit illustrates how mercury-free gold mining can have positive long-term implications for both gold miners and the environment," said library director Robert Weldon. He noted that among all the deserving exhibits displayed at TGMS, the GIA Library's stood out due to the

Figure 55. The GIA Museum's "Paint the Town Ruby Red" exhibit at TGMS featured a Burmese ruby and diamond necklace and earrings, courtesy of Mona Lee Nesseth (Custom Estate Jewels) and a private collector. Photo by Terri Ottaway.

Figure 56. The GIA Library's award-winning exhibit on mercury-free mining at the Tucson Gem and Mineral Show. Photo by Chris Rogers.

importance of responsible mining and sustainability in the industry.

In 2021, GIA provided a grant to Mercury Free Mining (MFM) and the Alliance for Responsible Mining (ARM). New methods for concentrating gold continue to be explored and tested with the goal of significantly reducing, or even eliminating, the use of mercury in gold mining.

Erica Zaidman
GIA, Carlsbad

ANNOUNCEMENTS

Sixth annual Gianmaria Buccellati Foundation Award winner. Sara Guergova, a graduate of GIA's Jewelry Design program in London, received the sixth annual Gianmaria Buccellati Foundation Award for Excellence in Jewelry Design. The 12 finalists and winner were announced at the GIA Alumni Collective's "Night at the Museum" event held during the AGTA GemFair in Tucson. Guergova, the first student from the London campus to win the award, designed a stunning bracelet featuring swans to represent togetherness and loyalty (figure 57).

Created in partnership with the Gianmaria Buccellati Foundation in 2018, the award recognizes outstanding talent in design among GIA students worldwide. Larry French, chief officer for North America strategies at the foundation, said, "On behalf of the Gianmaria Buccellati Foundation, we want to congratulate Ms. Sara Guergova, this year's winner, plus all the other finalists whose work so enriched this year's competition. We also want to recognize the talented GIA design instructors who helped guide the students on their way to the final judging in Tucson."

The 2023 Gianmaria Buccellati Foundation Award for Excellence in Jewelry Design competition is underway and open to students in GIA's Jewelry Design courses who meet the eligibility requirements. Visit www.gia.edu/buccellati-foundation-award-jewelry-design for more information.

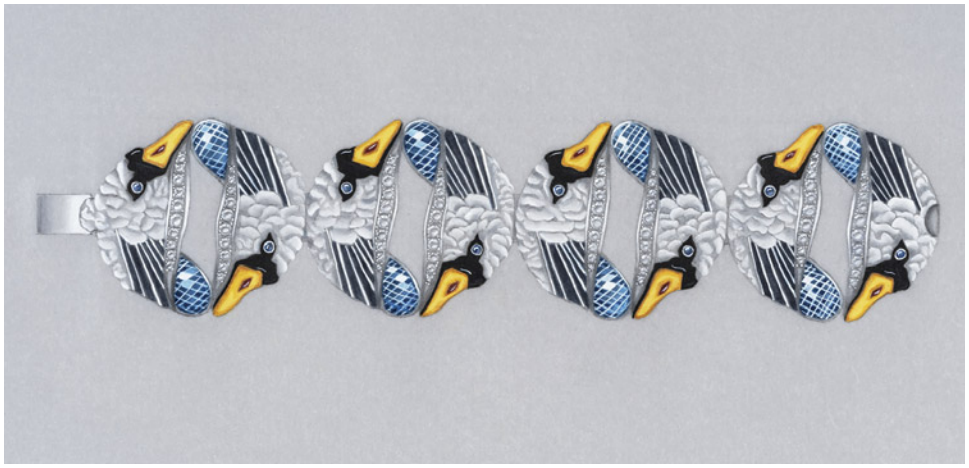

Figure 57. Sara Guergova's winning design sketch for the 2022 Gianmaria Buccellati Foundation Award for Excellence in Jewelry Design, featuring gold, black onyx, ruby, diamond, tourmaline, and blue sapphire.

2023 Tucson Photo Gallery

The pendant on the right is a miniature recreation of the "Bahia," a massive rutilated quartz fashioned by Glenn Lehrer and Lawrence Stoller. Each pendant in the collection is carved from leftover raw material. The photo on the left is by Harold and Erica Van Pelt; courtesy of Glenn Lehrer. The photo on the right and the rest of the photos in this gallery are by Robert Weldon.

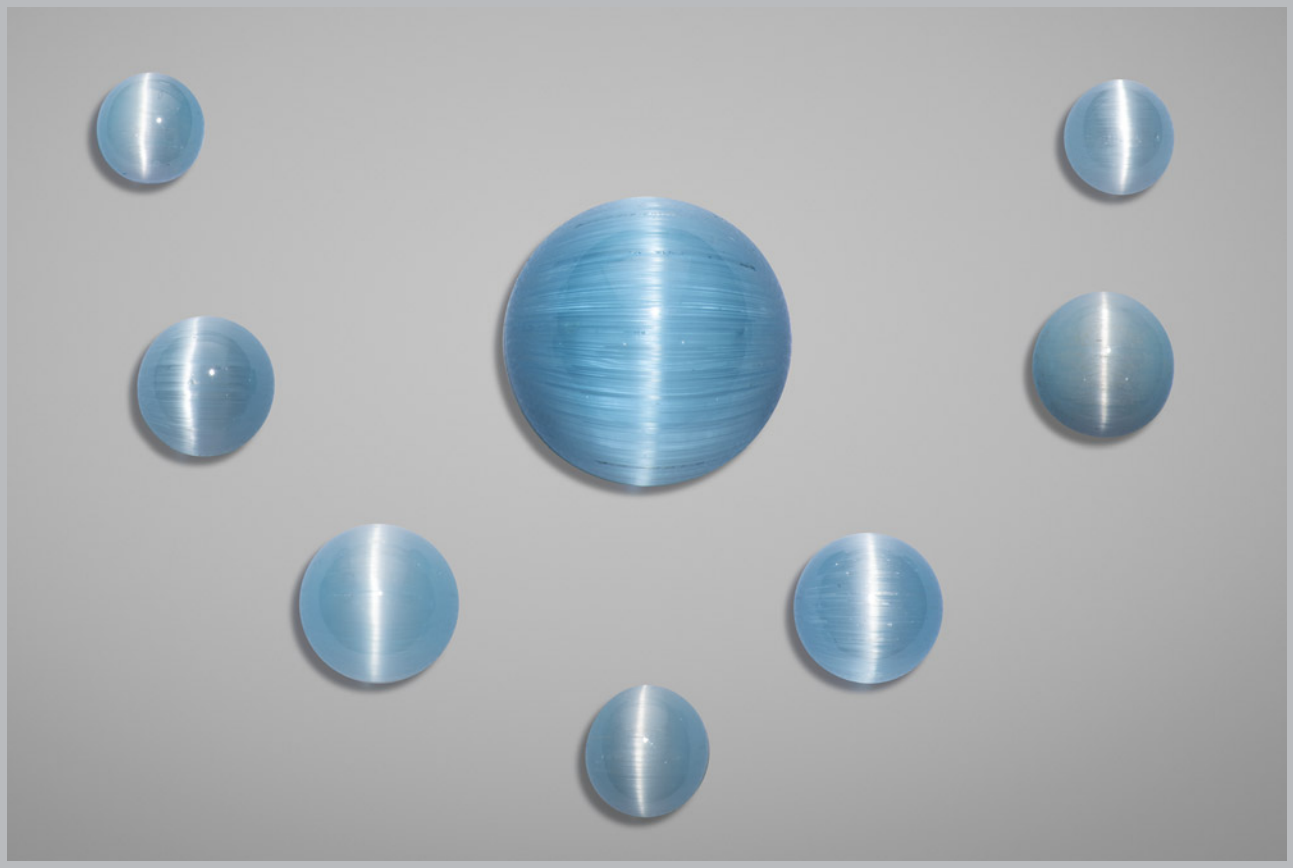

This suite of cat's-eye topaz cabochons of unknown origin features a 135.80 ct center stone. Courtesy of Mayer & Watt.

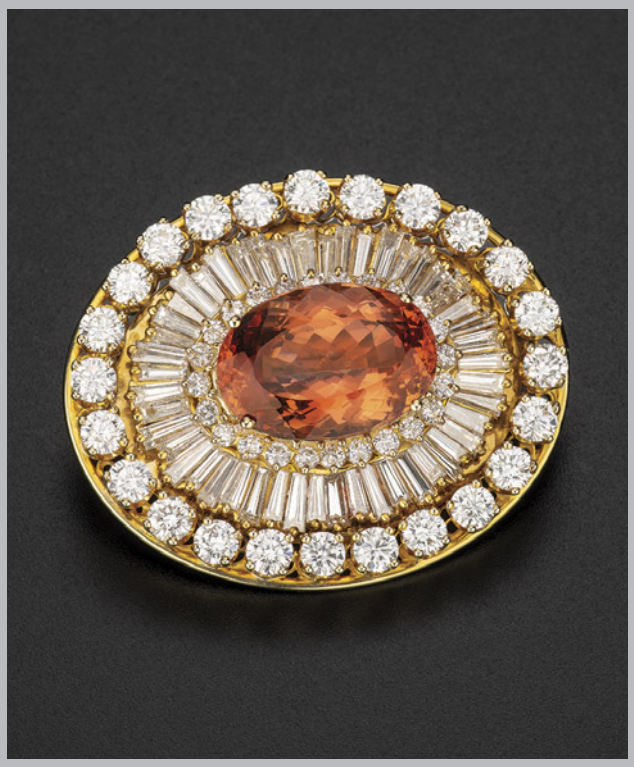

This brooch features a 13.27 ct Imperial topaz surrounded by 8.50 carats of diamonds, mounted in 18K yellow gold. Courtesy of Jewelerette & Co.

In this beautifully matched pair of natural pearl earrings, each 10 ct round pearl sits atop an astonishingly large 32 ct pearl drop. Courtesy of Sima G. Ltd.

A spray of "mango" quartz measuring 92 × 103 mm from the Boyacá Province in Colombia. The yellow coloration is believed to be due to the mineral halloysite. Courtesy of Cornerstone Minerals.

This naturally formed azurite disc on kaolinite matrix, accompanied by a cluster of malachite, hails from the Malbunka copper mine in Northern Territory, Australia. It measures 123 × 140 mm. Courtesy of Fine Art Minerals and Ghulam Mustafa.

A stunning pair of Alexandre Reza 18K gold earrings. In this design, 112 diamonds (totaling 7.86 carats) dangle from two emeralds (totaling 2.12 carats). Courtesy of Jardin Jewels.

Rough and carved hemimorphite, weighing 173.35 ct and 112.26 ct, respectively. Courtesy of Evan Caplan.

A vintage Fred of Paris demi-parure of earrings and a bangle, set with diamonds, rubies, emeralds, and sapphires. Courtesy of Jardin Jewels.

This aquamarine spray cluster from Skardu, Pakistan, measures 160 × 102 mm. Courtesy of Fine Art Minerals and Ghulam Mustafa.

Indicolite from Afghanistan. The 116.7 ct crystal is from Nuristan Province, and the 9.39 ct cut gem is from Kunav Province. Courtesy of Dudley Bauwet Gems and Mountain Minerals International.

Earrings and necklace in a jellyfish motif, set in 14K yellow gold. The mabe pearls are from the Sea of Cortez. Courtesy of Columbia Gem House.

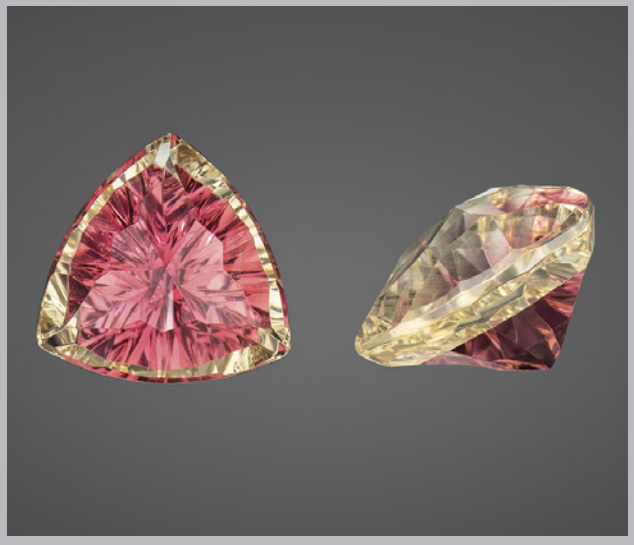

Master cutter Mark Gronlund combines natural Oregon sunstone with unheated Nigerian pink tourmaline in this 7.35 ct doublet, shown in table and profile views. Courtesy of Desert Sun Mining and Gems.

A Cartier Les Oiseaux Libérés diamond, emerald, and sapphire ring crafted in 18K white gold. Courtesy of Jardin Jewels.

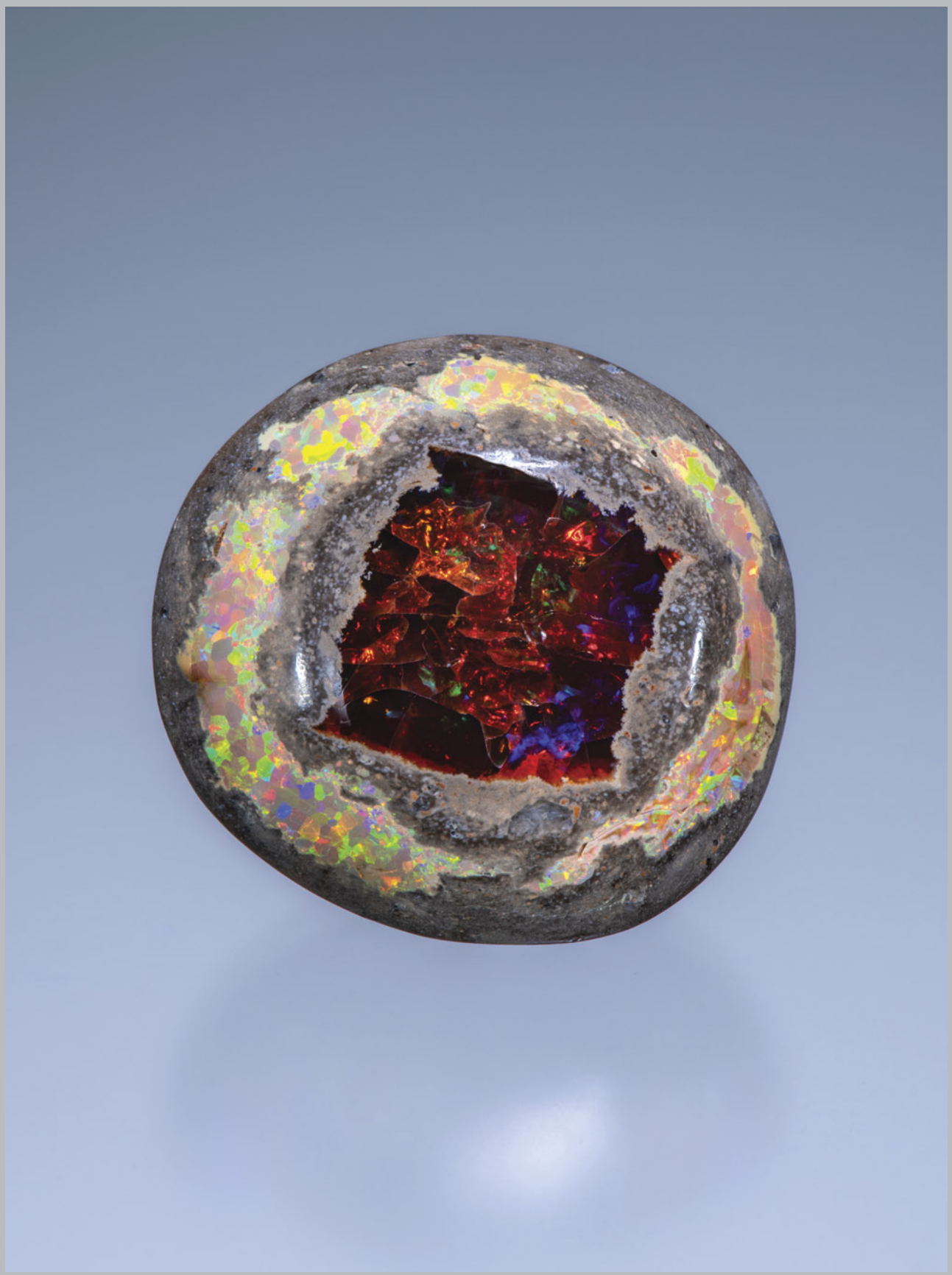

Aptly named the "Ring of Fire," this Ethiopian opal in matrix displays a square of dark opal surrounded by a ring of white opal. Courtesy of Ellie Gem Arts.

This bicolor spodumene is from Nuristan Province, Afghanistan. Terminations of the crystal appear to mimic the mountain range from which it was mined. Courtesy of Dudley Blauwet Gems and Mountain Minerals International.

Vintage diamond and carved emerald bracelet designed by Alexandre Reza. Courtesy of Jardin Jewels.

An art nouveau enameled necklace in a floral motif incorporating 20 seed pearls, four natural freshwater pearls, and a freshwater Mississippi dogtooth pearl. Courtesy of Bernard Nacht & Co./Under the Crown.

This horn-shaped boulder opal measures 75.5 × 15.9 × 4 mm and weighs 74.20 ct. Courtesy of Dufty Weis Opals Inc.

REGULAR FEATURES

COLORED STONES AND ORGANIC MATERIALS

***Pinctada radiata* atypical bead cultured pearls from the UAE.** Pearling is embedded in the culture and traditions of everyday life in the United Arab Emirates (UAE), especially in the trading center of Julfar. Abdulla Al Suwaidi, grandson of one of the last traditional pearl divers in the UAE, took on the challenge of reviving the country's pearling industry. He succeeded in establishing the Suwaidi Pearl Farm in Al Rams, Ras Al Khaimah (RAK), in 2005. Suwaidi's cultured pearl farm is recognized as the first of its kind in the Arabian (Persian) Gulf region.

GIA's Mumbai laboratory recently examined a quantity of cultured pearls obtained from the farm. The parcel contained variously shaped white to cream-colored pearls. Examination by real-time microradiography (RTX) showed a variety of different internal structures including bead and non-bead cultured pearls, but two pearls in particular (figure 58) revealed very interesting structures and were confirmed to be samples from atypical "bead" culturing experiments conducted by the farm. Pearl A was light cream and near-round, weighing 0.87 ct and measuring 5.13 × 4.93 mm, while pearl B was cream and button shaped, weighing 0.94 ct and measuring 5.42 × 5.12 × 4.93 mm. When viewed under 40× magnification, both pearls exhibited a smooth surface and possessed typical nacreous overlapping aragonite platelets.

Additional RTX and X-ray computed microtomography (μ-CT) analyses were conducted to further study the internal structures. RTX imaging of pearl A revealed a non-bead cultured pearl used as a "bead" nucleus (figure 59). A light gray core surrounded by organic-rich concentric growth structures followed by finer growth arcs was visible. An obvious demarcation with a small organic tail-like feature just below the surface overgrown with cultured nacre was also apparent. The lack of growth arcs in the nacreous layers was due to rapid growth during the culturing process ("Atypical 'beading' in the production of cultured pearls from Australian *Pinctada maxima*," *GIA Research News*, February 13, 2017). Similarly, pearl B revealed a natural pearl used as a "bead" nucleus (figure 60), with a very small but clearly visible dark gray core surrounded by faint growth arcs. As with pearl A, a distinct demarcation with organic-rich areas and a small organic tail-like feature were evident just below the surface overgrown with cultured nacre. X-ray computed microtomography analysis of both samples revealed clearer images of the demarcation between the "bead" pearls used as nuclei and the cultured nacre overgrowths.

Optical X-ray fluorescence examination did not show any fluorescence in either sample. Energy-dispersive X-ray fluorescence spectrometry revealed manganese levels below detection limits and strontium levels of 1130 ppm for pearl A and 1446 ppm for pearl B. The results from both testing methods were consistent with a saltwater growth environment. The ultraviolet/visible reflectance spectra collected for both pearls showed features around 435 and 460 nm and an additional weak band at 495 nm. These fea-

Figure 58. Two atypical bead cultured pearls recovered from Pinctada radiata *mollusks from Abdulla Al Suwaidi's farm in the UAE. Pearl A (left) weighs 0.87 ct, and pearl B (right) weighs 0.94 ct. Photo by Gaurav Bera.*

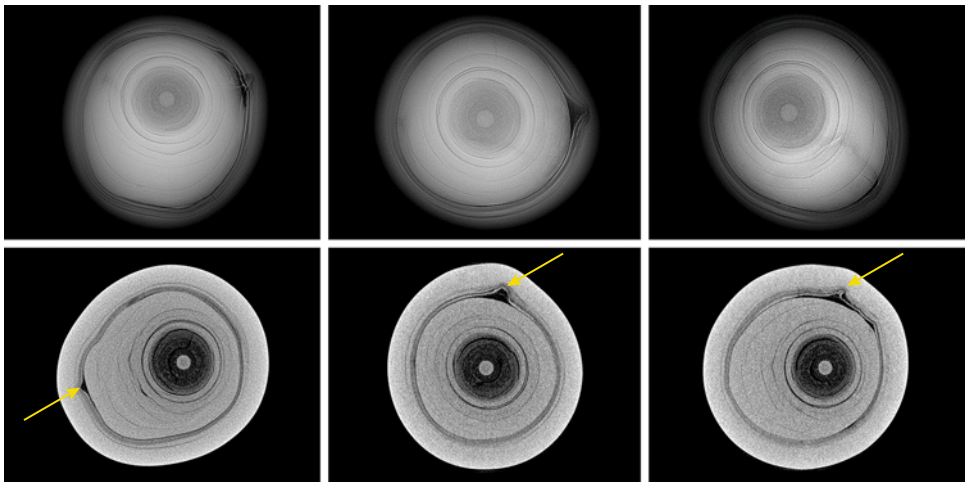

Figure 59. Top: RTX images in three directions of the non-bead cultured pearl used as a "bead" with a distinct demarcation and an organic tail-like feature in pearl A. Bottom: µ-CT scans of pearl A. The tail feature is indicated by a yellow arrow.

tures are similar to spectral observations previously recorded for natural *Pinctada radiata* pearls (A. Al-Alawi et al., "Saltwater cultured pearls from *Pinctada radiata* in Abu Dhabi (United Arab Emirates)," *Journal of Gemmology*, Vol. 37, No. 2, 2020, pp. 164–179). Raman analysis using 514 nm laser excitation was carried out on the surfaces of both pearls, and a doublet at 704/705 cm^{-1} as well as a peak at 1085 cm^{-1}, indicative of aragonite, were observed. Weak polyenic pigment-related peaks at 1130 and 1540 cm^{-1} were only observed for pearl B and were associated with its cream coloration. The photoluminescence spectra were also consistent with the Raman results and displayed high fluorescence together with the aragonite peaks, typical of most nacreous pearls.

Using lower-quality pearls (both nacreous and non-nacreous), gemstones, and other materials as "bead" nuclei has been a known practice for the last decade ("Chasing cultured pearls at SSEF: Cultured pearls using a natural pearl as a bead," 2020, https://www.ssef.ch/chasing-cultured-pearls-at-ssef-cultured-pearls-using-a-natural-pearl-as-a-bead/). Although not seen on a regular basis, atypical "bead" cultured pearls (aBCPs) are encountered in laboratories from time to time and can be very challenging to separate from some natural pearls. This would be especially true of the two samples featured in this report: If either of them were drilled and mixed in strands with natural Gulf pearls, an experienced gemologist would find it difficult to separate them from the other pearls. The authors have encountered natural pearls with similar distinct boundaries. It should also be noted that the aBCPs produced at the Suwaidi farm are the result of successful experiments, and they are not commercially available at the time of this writing. The farm continues to conduct various experiments and aims to restore the UAE's place in the global market by producing the finest *Pinctada radiata* cultured pearls available.

Abeer Al-Alawi
GIA, Global

Lubna Sahani
GIA, Mumbai

Nicholas Sturman
Bangkok

Chunhui Zhou
GIA, New York

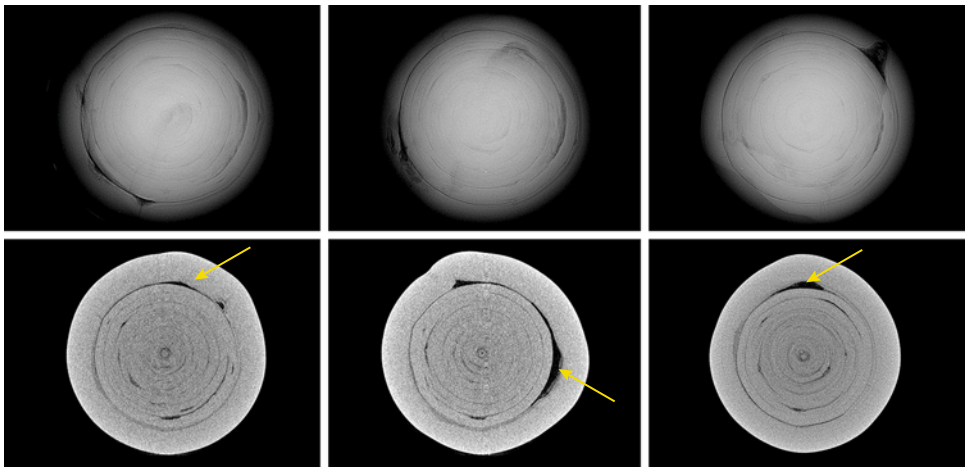

Figure 60. Top: RTX images in three directions of a natural pearl used as a "bead" with a clear demarcation and an organic tail-like feature in pearl B. Bottom: µ-CT scans of pearl B. The tail feature is indicated by a yellow arrow.

Figure 61. Twelve Chilean abalone cultured pearls and two red abalone (Haliotis rufescens) *shells with attached cultured shell blisters, as well as three 7 mm traditional freshwater shell bead nuclei used to culture the pearls. Photo by Emily Lane.*

Bead cultured abalone pearls from Chile. Abalone is the common name of the marine mollusk species that belongs to the *Haliotis* genus. Various abalone species are distributed worldwide along cold coastal waters. They live in rocky habitats, attaching firmly with their muscular foot. Abalone is highly prized for its meat, shell, and pearls. Due to a marked decrease of abalone populations, harvesting wild-caught abalone is heavily regulated. Thus, approximately 95% of the global abalone supply comes from farms around the world, in countries such as China, South Korea, South Africa, Chile, Australia, Taiwan, Japan, the United States, and New Zealand (P.A. Cook, "Worldwide abalone production statistics," *Journal of Shellfish Research*, Vol. 38, No. 2, 2019, pp. 401–404).

Abalone's ear-shaped shells and pearls are known for their unique, vibrant iridescent nacre, which is sought after in jewelry and decorative items. The iridescence phenomenon is also known as "orient," and it is attributed to interference and diffraction of light in the multilayered aragonite platelet microstructure and organic components. Due to the rarity of natural abalone pearls, most abalone products used in jewelry today are either abalone shells or assembled cultured shell blisters (also known as "mabe pearls").

The culturing of whole pearls in abalone mollusks started around the same time as shell blister culturing for producing mabe pearl (assembled cultured shell blister), and various methods have been attempted over the years (C.Y. Wentzell, "Cultured abalone blister pearls from New Zealand," Fall 1998 *G&G*, pp. 184–200; M. Monteforte and H. Bervera, "Abalone pearl culture on the west coast of the Baja California peninsula, Mexico," *World Aquaculture*, 2010, pp. 12–17). However, due to abalone's hemophilia and poor tolerance for chemicals and handling, any significant cut could cause major bleeding, and the nucleation and implantation procedures could induce infection that prohibits the mollusk from producing nacre. Therefore, the success rate of bead cultured (BC) abalone pearls was always low and the pearls were of unmarketable quality.

After 10 years of experimenting, scientists from the University of Antofagasta, Chile, have successfully created abalone BC pearls using a patented method for producing free pearls in abalone. Twelve of their cultured pearls and two abalone shells with a cultured shell blister attached (figure 61) were submitted to GIA for study in May 2022. They were the pilot crop of a new pearl culturing technique using traditional freshwater shell bead nuclei (5 to 8 mm) inserted into grafting channels in the visceral mass of *Haliotis rufescens* (red abalone) imported into Chile from Mexico in the 1990s (figure 62, left) for abalone farming. The BC pearl cultivation takes place during the last 24–28 months of the abalone culture process that usually takes 48–52 months, allowing the abalone meat and the pearl to be harvested at

Figure 62. Abalone mollusks were grown in an aquaculture recirculation system in eight raceways of 5000 liters. A local kelp species (shown on the right) was used to feed the mollusks twice per week. Photos courtesy of Jorge Donoso Mena.

the same time. The facilities include an aquaculture recirculation system in eight raceways of 5000 liters, with continuous aeration by blowers and a culture water flow of 5000 liters per hour (figure 62, right). The local kelp species *Lessonia trabeculata* obtained from natural, sustainably managed sources is used to feed the mollusks twice a week. Despite a high rate of bead nucleus rejection, the survival rate of the mollusks after grafting has been 99% and is currently at 15,000 grafted mollusks per trial, according to the farm.

The cultured abalone pearls produced using this method displayed multicolored nacreous surfaces due to strong iridescence, along with patches and stripes of dark brown organic materials. They exhibited a variety of baroque forms, and four samples possessed horn or tooth shapes often found in natural abalone pearls. A characteristic underlying botryoidal-like surface structure, usually observed on natural abalone pearls and shells, was also present (Fall 2015 Lab Notes, pp. 319–320). Real-time microradiography (RTX) revealed a round bead nucleus in the majority of samples, and the nacre layer thickness surrounding the bead nuclei ranged from 0.10 to 1.20 mm (figure 63). One sample lacked a bead nucleus and was

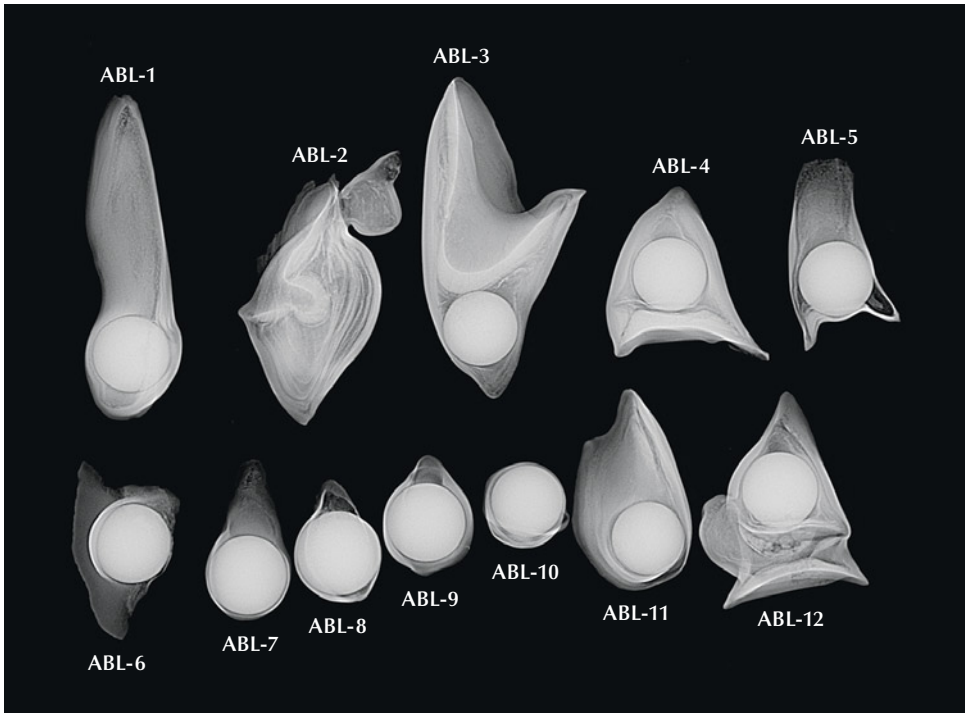

Figure 63. RTX images reveal 5–8 mm round shell bead nuclei in a majority of the abalone samples (ABL), with the nacre layer thickness surrounding the bead nuclei ranging from 0.10 to 1.20 mm. A bead nucleus was absent in sample 2, only showing layered growth with void-related features. While it is considered a non-bead cultured pearl, its internal structure resembled the internal structure commonly found in natural abalone baroque pearls. Image by Amiroh Steen.

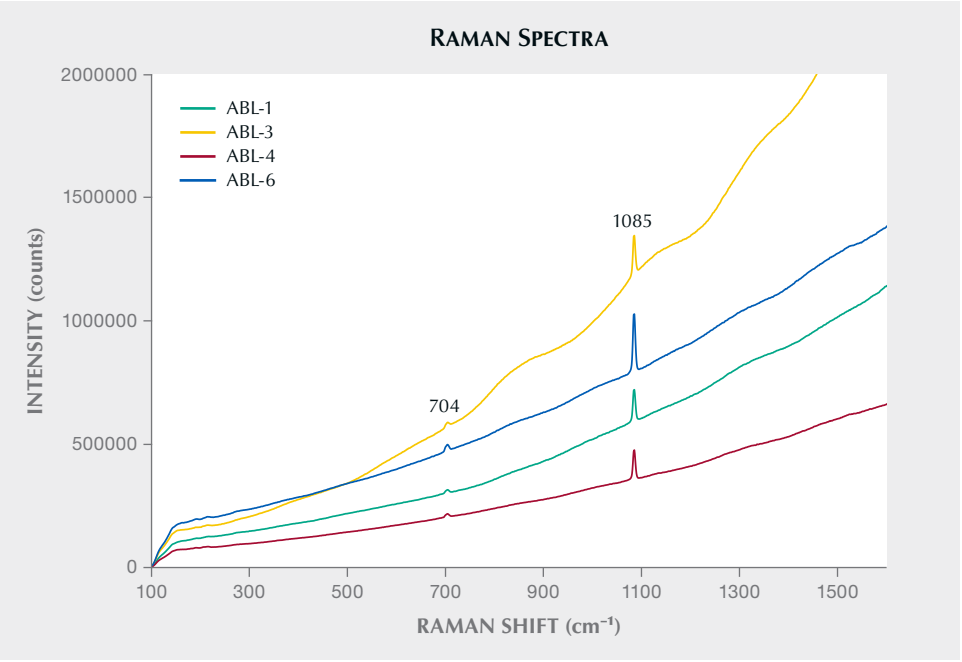

Figure 64. Raman spectra using 514 nm laser excitation showed high fluorescence background and weak peaks of aragonite displayed at 704 and 1085 cm^{-1}. These results are consistent with 10 natural abalone samples selected for preliminary comparison study.

identified as a non-bead cultured (NBC) pearl. Its layered growth with void-related features resembled the internal structure commonly found in natural abalone baroque pearls.

Ten natural abalone pearls were selected for spectroscopic and chemical comparison with the cultured pearl samples, and both types of samples showed similar results. No specific patterns were observed in ultraviolet/visible reflectance and photoluminescence spectra, and Raman spectra showed high fluorescence background and weak peaks of aragonite at 704 and 1085 cm^{-1} (figure 64). Energy-dispersive X-ray fluorescence analysis revealed all the samples had very low or below detection limit manganese content and high levels of strontium ranging from 1100 to 5000 ppm. High iodine levels were also detected in most samples, which is common in abalone. Trace element concentrations determined by laser ablation–inductively coupled plasma–mass spectrometry (LA-ICP-MS) were compositionally similar in both sample types. However, the cultured samples contained lower boron and higher potassium contents. All four tested spots of the NBC samples could be clearly separated from natural samples in the plot of boron vs. potassium contents (figure 65). Since the one NBC pearl showed an internal structure similar to that of natural abalone pearls, the plot can potentially be used to differentiate NBC pearls from natural samples. However, further study on both sample types is required. Additionally, all abalone samples showed higher strontium concentrations than *Pinctada* species previously studied.

The success of abalone BC pearl production could be a promising addition to the gem and jewelry industry, and this study provided useful information for future reference.

Figure 65. The cultured and natural abalone pearl samples were compositionally similar in trace element concentrations determined by LA-ICP-MS. However, the cultured samples contained lower boron and higher potassium than the natural pearls. All four tested spots of the NBC samples are clearly separated from natural samples in this plot.

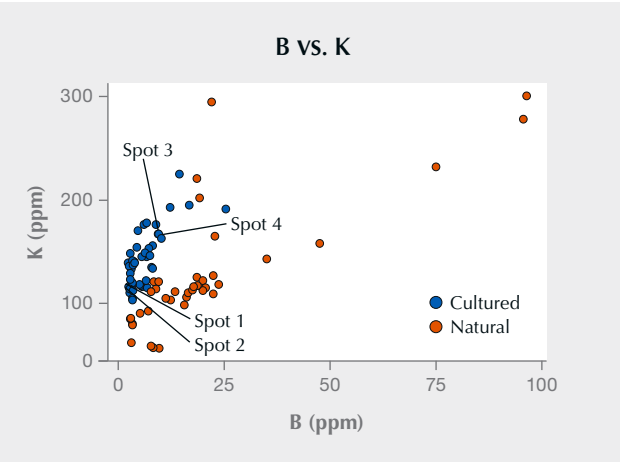

Artitaya Homkrajae, Amiroh Steen, Matthew Hardman, and Ziyin Sun
GIA, Carlsbad

Rubén Araya Valencia
Alexander von Humboldt Institute of Natural Sciences, University of Antofagasta

Jaime Pablo Maturana Zuñiga
Abalone Pearl Technology (APT SpA)
Antofagasta, Chile

Figure 66. Two natural pearls recovered from Pinctada radiata *mollusks by Bahraini divers, weighing 0.06 ct (pearl A, left) and 0.25 ct (pearl B, right). Photo by Gaurav Bera.*

Microscopic shells in natural pearls from *Pinctada radiata*. For centuries, natural pearl diving was Bahrain's main industry. The vast majority of natural pearls fished around the islands of Bahrain are found in the *Pinctada radiata* bivalve (known in Arabic as *mahar*). These pearl beds have been known to produce the finest-quality natural pearls in the Arabian (Persian) Gulf region. Given the Gulf's strategic trading location and the richness of its pearling industry, the pearls from this region are coveted by traders and collectors alike (R. Carter, "The history and prehistory of pearling in the Persian Gulf," *Journal of the Economic and Social History of the Orient*, Vol. 48, No. 2, 2005, pp. 139–209). GIA's Mumbai laboratory recently examined a quantity of these pearls obtained from two local Bahraini divers who claimed they were recovered from wild mollusks living in the nutrient-rich shallow waters off the coast of Sitra, one of Bahrain's 33 islands.

Natural pearls from *Pinctada radiata* fished from Bahrain and the Gulf region in general have a wide range of shapes and colors. While most of the pearls examined showed a variety of interesting internal structures, two of them had a noteworthy feature: a minute shell contained within. Natural pearls are very rare and form inside mollusk shells, and a shell within a pearl within a shell is like nature's version of a nesting doll. Such structures have been encountered by GIA on rare occasion (see Winter 2015 Lab Notes, pp. 434–436).

Both pearls were very small (figure 66). The smaller one (A) had a strong yellow bodycolor and an oval shape, weighing 0.06 ct and measuring 2.07 × 1.93 mm. The larger round one (B) had a light cream color, weighing 0.25 ct and measuring 3.30 mm in diameter. When viewed under 40× magnification, both exhibited typical nacreous overlapping aragonite platelets. Real-time microradiography (RTX) and X-ray computed microtomography (μ-CT) analyses were carried out to examine the internal structures in greater detail.

A minute gastropod shell measuring approximately 0.50 × 0.30 mm was observed in pearl A. The shell walls were very thin, and minimal growth arcs were present in the nacre surrounding it (figure 67). Marine gastropods are known to range in size from a few millimeters to more than a meter, so the size of the shell inside this pearl suggests it was from a juvenile gastropod just beginning to form its shell. The juvenile shell later forms the protoconch or first whorls of an adult gastropod (A. Nutzel, "Larval ecology and morphology in fossil gastropods," *Paleontology*, Vol. 57, Part 3, 2014, pp. 479–503).

RTX imaging of pearl B revealed a minute shell that appeared to be a foraminifera test (shell), measuring approximately 0.45 × 0.35 mm. Foraminifera are small unicellular marine organisms found on the sea floor. A thin layer of organic matter that appeared darker in the RTX and μ-CT images seemed to envelop the foraminifera test, and a few growth arcs were observed within the surrounding nacre (figure 68). The μ-CT scan was also rendered using specialized software (C. Zhou et al., "New 3-D software expands GIA's pearl identification capabilities," *GIA Research News*, May 13, 2016) to create a three-dimensional image that

Figure 67. The gastropod shell, measuring approximately 0.50 × 0.30 mm, observed in pearl A. A: RTX image of the shell. B–D: μ-CT scans of the shell in the X, Y, and Z directions, respectively. (The weak white rings on the lower right image are artifacts and not pearl-related structures.)

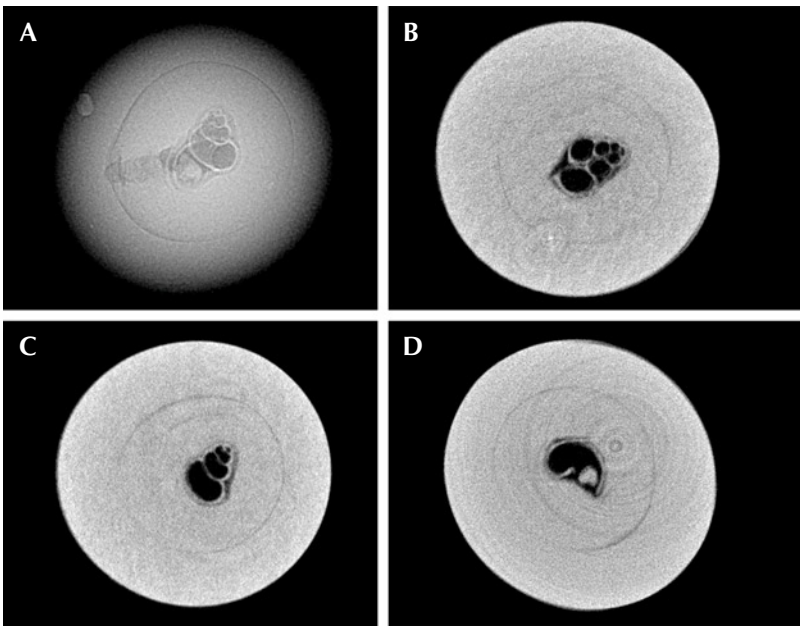

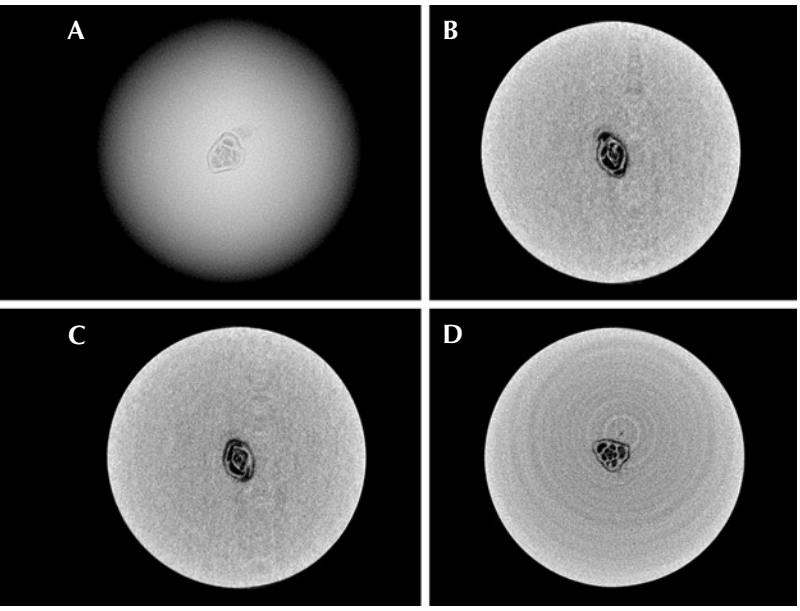

Figure 68. The foraminifera test, measuring approximately 0.45 × 0.35 mm, observed in pearl B. A: RTX image of the foraminifera test. B–D: µ-CT scans of the foraminifera test in the X, Y, and Z directions, respectively. (Again, the weak white rings on the lower right image are artifacts.)

made it easier to see the external morphology of the shell within the pearl (figure 69). The foraminifera test appeared multilocular, or multichambered, with tubular chambers arranged around a growth axis to form a beautiful milioline arrangement of chambers (A.R. Loeblich and H. Tappan, *Foraminiferal Genera and Their Classification*, Springer, New York, 1988). The minute size of the shells within these tiny pearls is a good indicator of their natural origin.

Energy-dispersive X-ray fluorescence spectrometry on pearls A and B revealed low manganese levels of 39.0 ppm and 17.8 ppm and high strontium levels of 1768 ppm and 1497 ppm, respectively, which is characteristic of formation in a saltwater environment. Raman analysis was also carried out using 514 nm laser excitation on the surface of each pearl. A doublet at 702 and 705 cm^{-1} as well as a peak at 1085 cm^{-1} indicative of aragonite were observed, along with minor polyenic pigment peaks at 1130 and 1530 cm^{-1}. Photoluminescence (PL) spectra were also collected on both pearls. Pearl A revealed three broad peaks at 620, 650, and 680 nm, characteristic of many naturally colored pearls, while pearl B showed clear aragonite peaks and low fluorescence. An ultraviolet/visible reflectance spectrum was collected only for pearl B within the 220–850 nm range, as pearl A's size prevented the detector from obtaining a clear result. Faint features at 420 and 495 nm were, like the PL results, consistent with natural coloration. Similar spectral observations have previously been documented in natural *Pinctada radiata* pearls (A. Al-Alawi et al., "Saltwater cultured pearls from *Pinctada radiata* in Abu Dhabi (United Arab Emirates)," *Journal of Gemmology*, Vol. 37, No. 2, 2020, pp. 164–179).

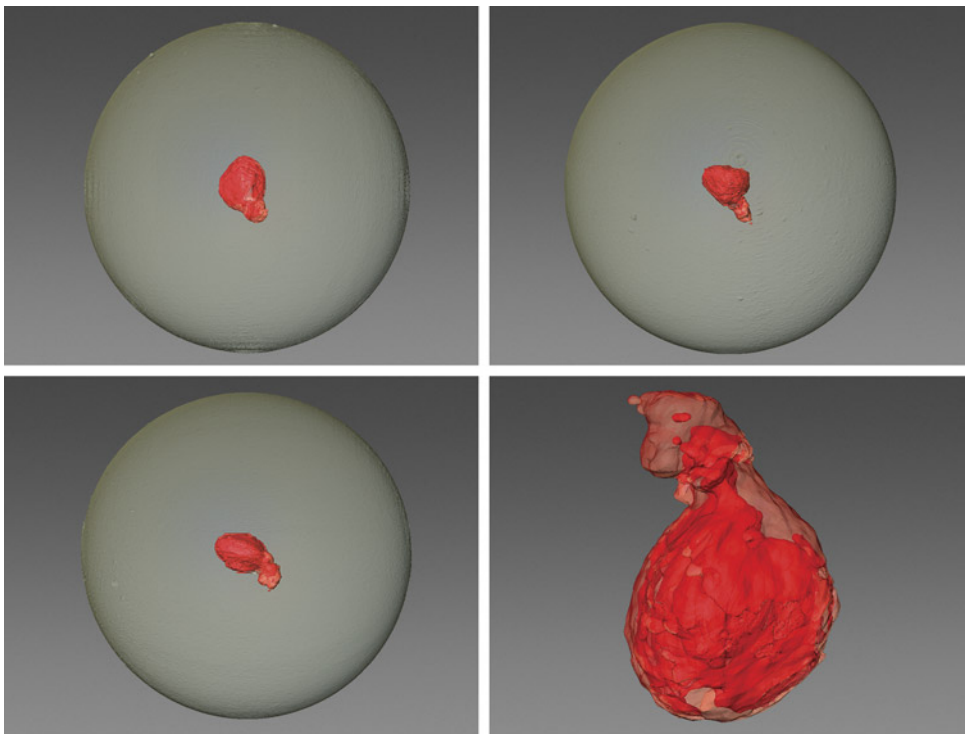

Figure 69. 3D images constructed from µ-CT scans of pearl B illustrate the morphology of the foraminifera test. Images by Emiko Yazawa.

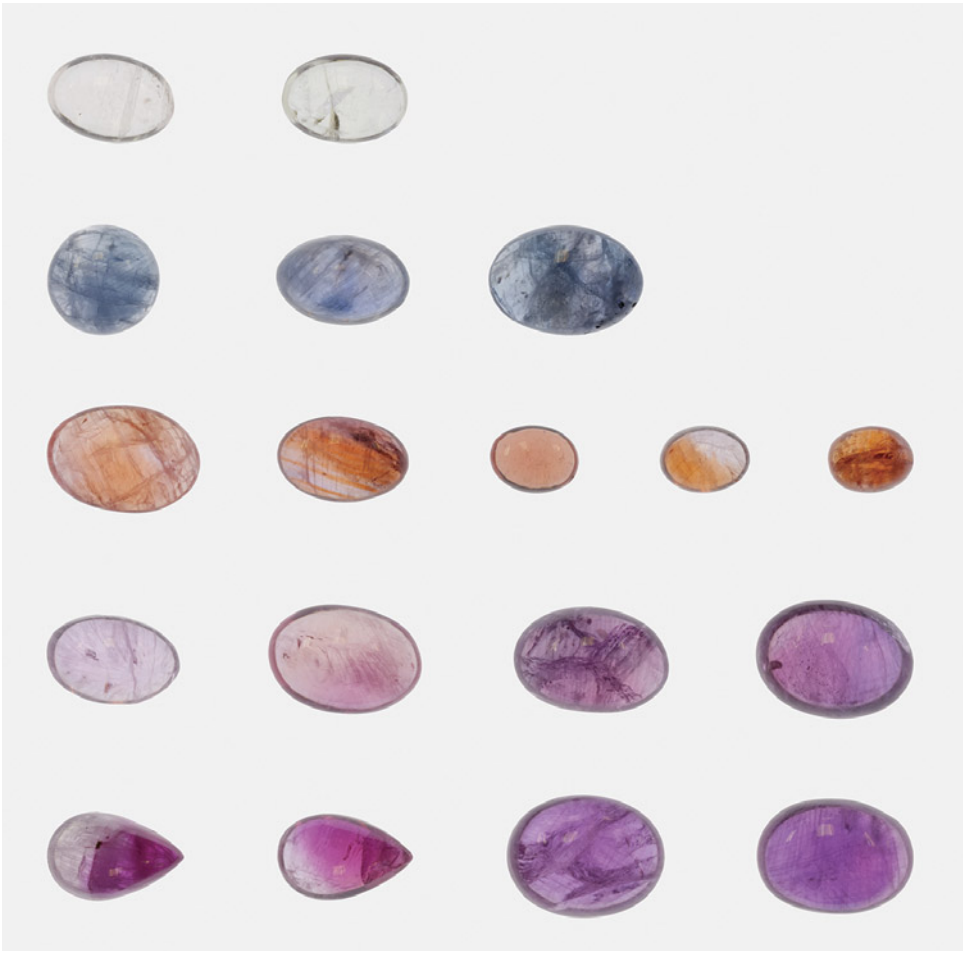

Figure 70. Part of the suite of sapphires studied for this project (weighing 0.23–1.41 ct). Photo by Sasithorn Engniwat; courtesy of Greenland Ruby.

The gemological examination of these *Pinctada radiata* pearls proved very rewarding, especially with regard to their internal structures. Research into what causes the formation of a pearl in the wild is ongoing. Hence, finding these minute shells that may be the initiation of growth in these two natural pearls is a truly rare circumstance.

Nishka Vaz
GIA, Mumbai

Nicholas Sturman
Bangkok

Abeer Al-Alawi
GIA, Global

Color study of fancy sapphire from Greenland. Over the past 70 years, several ruby and pink sapphire localities have been documented in the region of Greenland's capital city, Nuuk (P.W.U. Appel and M. Ghisler, "Ruby- and sapphirine-bearing mineral occurrences in the Fiskenaesset, Nuuk and Maniitsoq regions, West Greenland," GEUS, Geological Survey of Denmark and Greenland, 2014). Several of these localities are currently exploited on a small scale by the local communities. In 2017, Greenland Ruby A/S started a large-scale mining operation at the Aappaluttoq ruby and pink sapphire deposit, located 160 km south of Nuuk.

The corundum extracted at Aappaluttoq is heated in air at temperatures over 1500°C for several hours, with some flux added. In rare cases, the heating significantly alters the color of light pink and near-colorless sapphire, resulting in fancy-color sapphire. GIA recently studied a parcel of 22 of these fancy-color sapphires mined and treated by Greenland Ruby (figure 70).

A combination of ultraviolet/visible/near-infrared (UV-Vis-NIR) spectra and trace element chemistry using laser ablation–inductively coupled plasma–mass spectrometry (LA-ICP-MS) were collected at GIA in Bangkok to identify the causes of color. For full quantification of the chromophores, it is necessary to do this analysis in oriented, clean samples with a known path length. Since most of the Greenland material is polished as cabochons and contains some inclusions, it is very challenging to calculate or even estimate the absorption coefficients. We limited ourselves to a rough interpretation of the chromophores based on the shape of the spectra. Orientation of the samples was estimated based on the pleochroism.

Additionally, we could not precisely identify which area of the stone was analyzed during the spectroscopy, and

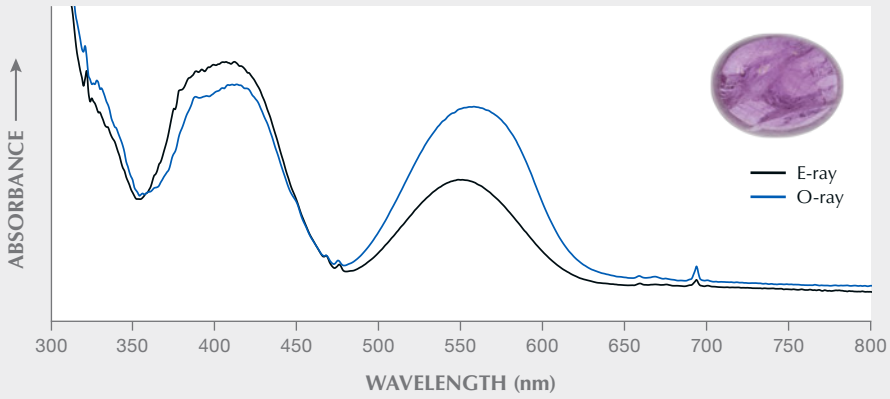

	Mg	Ti	V	Cr	Fe	Ga	[Ti]-[Mg]
S269663 Spot 2	33	36	26	283	500	11	3
S269663 Spot 3	34	35	26	287	508	11	1
S269663 Spot 4	37	39	26	268	478	11	2
Detection limits (ppma)	0.011	0.033	0.004	0.068	0.824	0.002	

Figure 71. A UV-Vis-NIR spectrum dominated by Cr^{3+} features often results in a pink to red stone, depending on the concentration of Cr^{3+} (in ppma). When the sample is oriented down the c-axis, the color often trends toward reddish purple (i.e., fancy sapphire).

thus all UV-Vis spectra were bulk measurements and combined the color of different zones. In contrast, the LA-ICP-MS analysis was performed at very specific spots, allowing the analysis of specific zones.

The literature describes six chromophores responsible for color in natural corundum (E.V. Dubinsky et al., "A quantitative description of the causes of color in corundum," Spring 2020 *G&G*, pp. 2–28). Four of the chromophores from that study are responsible for the colors in this suite.

Most stones from the Aappaluttoq deposit are colored by the Cr^{3+} chromophore, giving them their typical pink to red color (figure 71). The intensity of the color is directly linked to the concentration of Cr^{3+}, which can go up to several 1000 ppma, and in exceptional cases even to 15,000 ppma. Most of the lighter-colored material has a concentration of a few 100 ppma, resulting in a pink color.

Depending on the orientation, it can appear more purple (when viewed through the *c*-axis). In some cases, this is so strong that the face-up color of the stone is modified to an extent that it cannot be defined as ruby or pink sapphire and falls into the fancy reddish purple range. Some of the stones develop a more orangy tone after treatment. (A bright orange oval brilliant seen at the 2023 Tucson shows is highlighted on pp. 115–116 of this issue.) This color can be attributed to the creation of trapped holes in combination with Cr^{3+} (figure 72).

To create trapped holes, the chemical balance in the stone needs to be correct. Only when a stone is acceptor dominated will trapped holes be present. In the case of Greenland ruby, this comes down to the balance between Mg^{2+} vs. Ti^{4+}, Si^{4+}, and H^{+}. Since the stones have all been treated in air (oxidizing atmosphere), we can assume that H^{+} has diffused out of them. With the method used to measure trace elements (LA-ICP-MS with a quadrupole MS), we cannot correctly quantify the Si^{4+} content in these stones. The possibility that Si^{4+} plays a role in the color cannot be excluded. Regardless, there is no indication here that Si^{4+} is required to tilt the balance of chromophores when comparing trace elements vs. observed color. Since we do not aim to quantitatively analyze the color, we ignore any potential presence of Si^{4+}. This means that the concentrations of Mg^{2+} and Ti^{4+} are the determining factors: Only if the amount of Mg^{2+} is larger than the Ti^{4+} concentration can trapped holes develop in sapphire from Greenland.

Two ions in sapphire can pair with trapped holes: Fe^{3+} and Cr^{3+}. Since the trapped hole preferentially pairs with Cr^{3+}, this is the chromophore observed in these stones. The quantity of trapped holes that can form in corundum is very low, and as such, not all the Cr^{3+} couples with a trapped hole. The final color will be a combination of the trapped hole color and the pure Cr^{3+} chromophore, resulting in a combination of pink to red and orange colors. Trapped holes are very strong coloring agents that can have a major impact even when their concentration is very low.

The Fe^{3+} chromophore is the weakest one encountered in natural corundum. Very high concentrations of Fe^{3+} are required to create a yellow color, often exceeding several thousand ppma. Since the Greenland rubies have a maximum iron concentration under 1500 ppma, this chro-

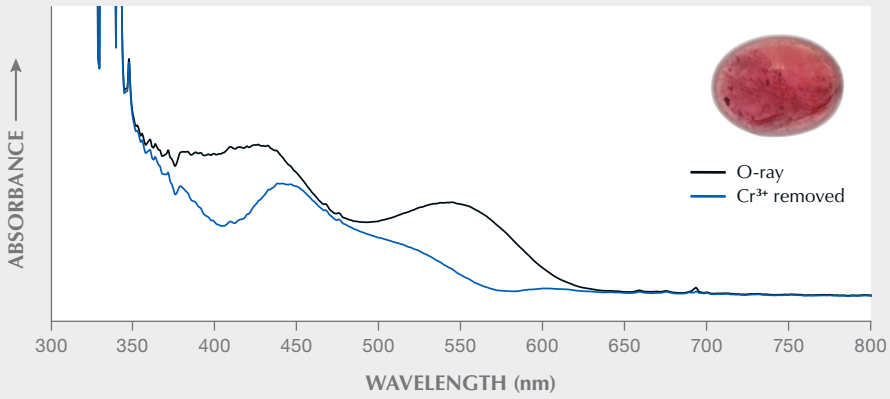

	Mg	Ti	V	Cr	Fe	Ga	[Ti]-[Mg]
S269596 Spot 1	31	13	15	820	924	12	–18
S269596 Spot 2	31	13	15	804	927	12	–18
S269596 Spot 3	32	13	16	812	971	12	–19
Detection limits (ppma)	0.011	0.033	0.004	0.068	0.824	0.002	

Figure 72. The peaks at 550 and 430 nm in the o-ray spectrum (black) suggest the presence of Cr^{3+}, causing pink to red in the stone. The trace element analysis (in ppma) shows a clear excess of Mg^{2+} compared to the Ti concentration, highlighting that trapped hole creation is very likely. When we remove the absorbance spectrum of Cr^{3+} from the stone's absorption spectrum (blue), it is obvious that the combination of Cr^{3+} with the trapped hole is the cause of the remaining color and the strong orange tint observed in the stone.

mophore creates only a very weak yellow color (figure 73). Other common chromophores are much stronger and more common, which makes it very difficult to notice any color contribution by Fe^{3+}. Only when the Cr^{3+} concentration is

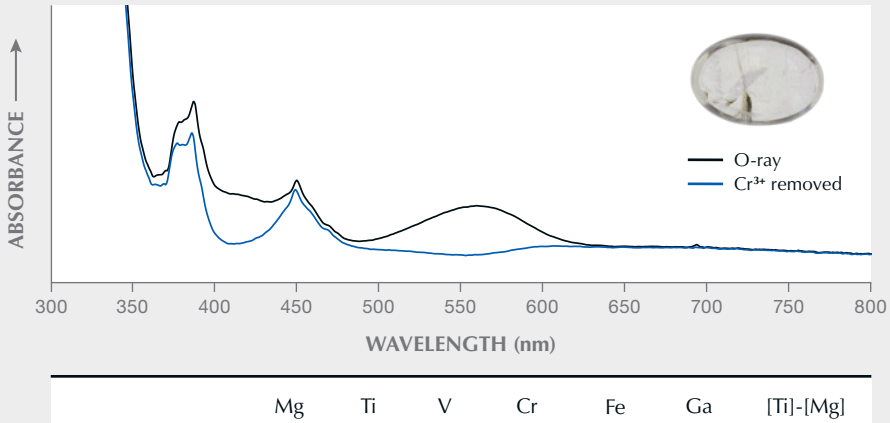

	Mg	Ti	V	Cr	Fe	Ga	[Ti]-[Mg]
S269612 Spot 1	16	14	10	96	1150	12	–2
S269612 Spot 2	13	12	9	81	1136	13	–1
S269612 Spot 3	14	12	9	76	1143	14	–2
Detection limits (ppma)	0.011	0.033	0.004	0.068	0.824	0.002	

Figure 73. This plot shows the o-ray spectrum of a pale yellow sample (black) and a modified o-ray spectrum where some contribution by Cr^{3+} is subtracted (blue). When the Cr^{3+} spectrum is removed, a pure Fe^{3+} spectrum remains. This spectrum is characterized by the double peak at 377–388 nm and one at 450 nm. The ratio of the 388 to 377 nm band suggests a relatively low Fe^{3+} chromophore concentration, which matches the observed color and analyzed chemistry (in ppma).

extremely low can we detect the pale yellow color from the Fe^{3+} chromophore.

The Fe^{2+}-Ti^{4+} chromophore creates a blue color in corundum and is relatively strong (figure 74). When observed in ruby from Greenland, its effect is usually limited to a slightly increased purplish hue in the chromium-rich corundum, occasionally modifying the color to a dominant purple hue. Only when the Cr^{3+} concentrations are extremely low is there a chance for the corundum to have a blue color. We still observe some cloudiness after the treatment in the blue zones.

We assume that this type of rough corundum had a milky appearance caused by a high concentration of fine rutile particles before treatment. During treatment at temperatures over 1200°C, some of the particles dissolved into the lattice, becoming available to pair with Fe^{2+} that was already present and creating a blue bodycolor. Due to the large amounts of Ti^{4+} that diffused into the crystal lattice, the iron was forced to remain in a reduced state (Fe^{2+}).

The nature of the treated corundum from Greenland makes high-quality spectroscopy a challenge. Nevertheless, we were able to isolate and identify the chromophores responsible for the fancy colors observed in these sapphires.

It is important to note that many of these fancy colors developed as a result of heat treatment. The trapped hole–related chromophores only become visible after H^+ diffused out of the stone under oxidizing conditions. These same conditions also allow the iron to oxidize and create the pale yellow color by Fe^{3+} chromophores. The high temperatures were also required to dissolve rutile particles into the corundum lattice and form Fe-Ti pairs.

While these fancy-color stones remain a curiosity, they make for a welcome addition from a mine that is known for its ruby and pink sapphires.

Wim Vertriest, Charuwan Khowpong, and Polthep Sakpanish
GIA, Bangkok

Martin Viala
Greenland Ruby

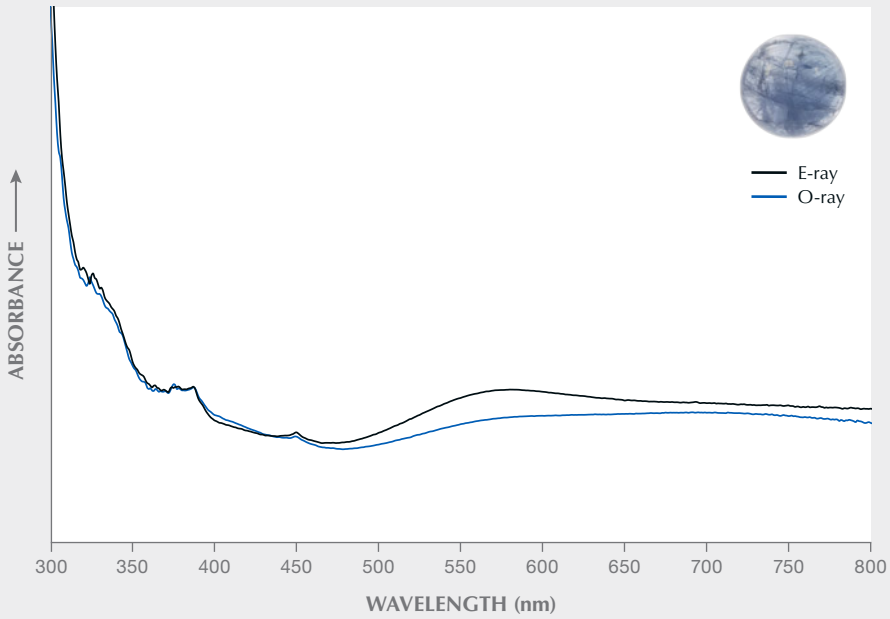

	Mg	Ti	V	Cr	Fe	Ga	[Ti]-[Mg]
S108627 Spot 1	46	120	15	21	544	10	74
S108627 Spot 2	38	54	14	39	548	11	16
S108627 Spot 3	47	52	16	40	613	11	5
Detection limits (ppma)	0.011	0.033	0.004	0.068	0.824	0.002	

Figure 74. The extremely low Cr^{3+} contents allow other features to be dominant. In this case, Fe^{2+}-Ti^{4+} charge transfers with a large peak at 580–620 nm are responsible for a blue color. The absorption spectrum of the stone also shows some features related to Fe^{3+}, which is a very weak chromophore and does not influence the color.

Figure 75. A handful of gem gravel collected from the Lofa River in Weasua, Liberia, showing the high concentration of ruby material. Photo courtesy of Diamonds for Peace.

Liberian ruby. A gemological education can often prove useful in the most unusual of circumstances. On a recent trip to rural Liberia with the Japan-based NGO Diamonds for Peace (DfP), the author discovered a previously unacknowledged source of ruby. The original purpose of the visit was to deliver a rough diamond grading and valuation workshop to the miners working and living in 17 communities across Liberia. During the trip, the author stayed in the town of Weasua, one of the larger mining communities, to experience the standard of living and the general working conditions of the miners. The poverty is extreme. Most homes are without electricity, facilities, or running water, and only three functional water pumps exist for a population of 5,000, all of which place the health and the well-being of this community at risk. DfP has been working with this community since 2018 and has made significant inroads in supporting and improving the lives of these miners, but there is a long way to go, and strategies to aid their mission are continually being developed.

It was therefore fortuitous that during the visit, the author learned that there were other promising gem-quality minerals in the alluvial gravels the miners were collecting in their pursuit of diamond (figure 75). Upon initial inspection while on-site, the author noted material resembling corundum (primarily ruby), garnet, topaz, rock crystal quartz, and possible spinel. Samples were purchased from the miners for analysis, which came as a welcome surprise since they were unaware that these colored stones could carry any value (figure 76, left).

The author subsequently analyzed all the samples at the Gemmological Certification Services (GCS) laboratory in London. Using advanced and standard gemological testing, the identity of all the presumed gem-quality minerals of the collected specimens was confirmed. Particular focus was placed on the rubies due to their apparent abundance at the mine site, with the hope of providing another means of income for this community.

All ten samples tested were identified as corundum. Due to the nature of the rough material, standard testing was limited, beyond measuring specific gravity—which, averaging 4.0 across all samples, supported corundum. The ultraviolet/visible/infrared absorption spectrum, with its chromium-associated features, was also consistent with ruby. X-ray fluorescence analysis of the trace element chemistry revealed 1029–2377 ppm iron and 721–2915 ppm chromium, with low levels of gallium (54 ppm) and vanadium (53 ppm).

Generally, the color of the alluvial material collected ranged from pinkish gray to a deep purplish red, with sizes varying from 6 to 14 mm (1.45–15.90 ct), although the au-

Figure 76. Left: One of the Liberian diamond miners displays some of the rubies she found while digging. Right: A ring mounted with a Liberian ruby. Photos by Diamonds for Peace (left) and Alex Herbert (right).

thor was shown larger pieces on-site. All of the material showed a moderate to weak red fluorescence response in long-wave UV and inert to weak red in short-wave UV, consistent with high-iron ruby due to the quenching of Cr^{3+}-associated fluorescence by iron. The majority of the samples showed lamellar twinning, surface-reaching fractures, and iron staining. The material was translucent to opaque, meaning that clear observation of any other inclusions was limited.

Although the material is not considered high-quality ruby, some of the better pieces have been polished to create attractive cabochons (figure 76, right). Diamonds for Peace is currently developing a business plan to monetize this material for the benefit of the community. The GCS laboratory will continue to support Diamonds for Peace as that organization explores this new potential avenue of income for the miners of Weasua.

Beth West
Gemmological Certification Services, London

Forsterite in a purple Tanzanian spinel. Purple/violet spinel from Tanzania is popular in the gem market today. Recently, author JW encountered an oval-shaped purple gemstone reportedly from Tanzania (figure 77). Its refractive index of 1.714 and hydrostatic specific gravity of 3.59

Figure 77. This faceted purple spinel, weighing 0.51 ct and measuring 5.20 × 4.17 × 3.10 mm, was reportedly from Tanzania. Photo by Jinlin Wu.

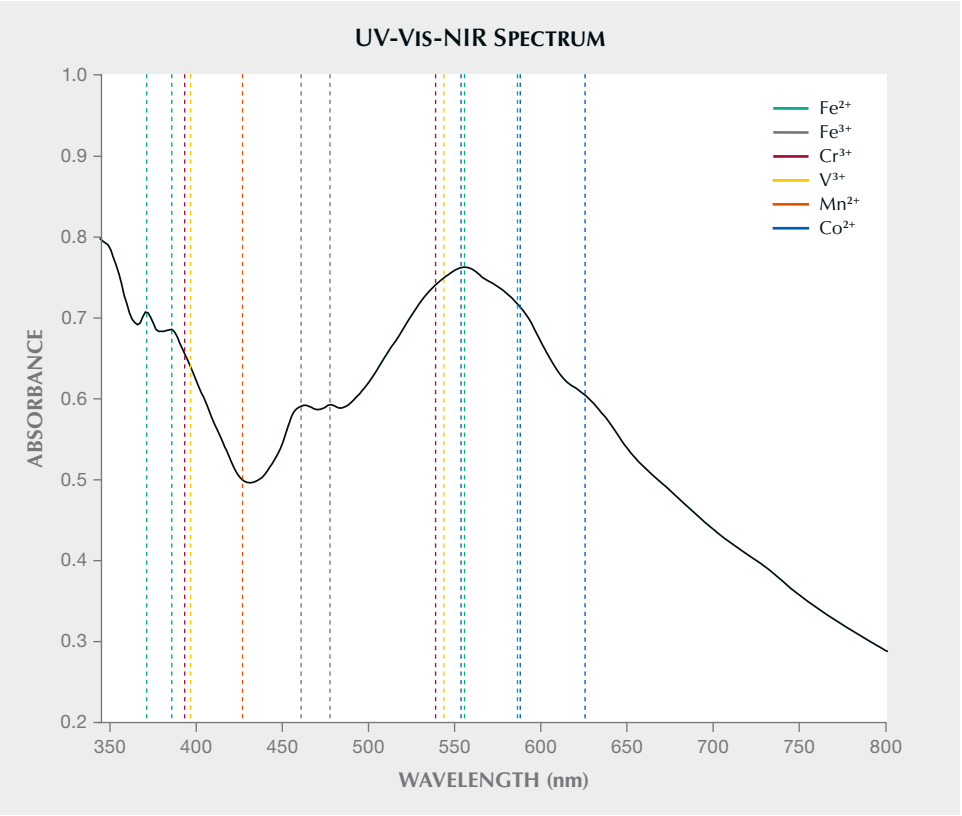

Figure 78. The UV-Vis-NIR spectrum of the spinel sample shows absorption peaks mainly related to Fe^{2+} and Fe^{3+}.

indicated spinel. Its ultraviolet/visible/near-infrared (UV-Vis-NIR) absorption spectrum was characterized by a series of absorption bands centered at 555 nm and several iron-related small bands centered at around 371, 385, 461, and 478 nm, as well as an extremely weak band at ~625 nm for Co^{2+} (figure 78). This absorption profile revealed that iron (Fe^{2+} and Fe^{3+}) was the main coloring element (P.M. Belley and A.C. Palke, "Purple gem spinel from Vietnam and Afghanistan: Comparison of trace element chemistry, cause of color, and inclusions," Fall 2021 *G&G*, pp. 228–238).

Energy-dispersive X-ray fluorescence analysis was performed to determine the sample's trace element concentration, which showed 10950 ppmw iron, 963 ppmw zinc, 52 ppmw chromium, 94 ppmw vanadium, and 9 ppmw cobalt. These results were similar to the chemical features of representative purple Tanzanian spinel: extremely high iron content, medium zinc content, and low chromium and vanadium contents (G. Giuliani et al., "Pink and red spinels in marble: Trace elements, oxygen isotopes, and sources," *Canadian Mineralogist*, Vol. 55, No. 4, 2017, pp. 743–761).

Microscopic observation revealed a colorless subhedral mineral, a dolomite with an unknown dark material attached (figure 79), and oriented short needles (figure 80). Raman spectroscopy identified the colorless mineral as forsterite. According to the RRUFF database (B. Lafuente et al., https://rruff.info/about/downloads/HMC1-30.pdf), peaks at 822, 855, 918, and 963 cm^{-1} were consistent with the main peaks of forsterite (figure 81).

As a rock-forming mineral, forsterite (Mg_2SiO_4) itself is common, especially in marble-hosted spinel. However, it is rarely observed in Tanzanian spinel and has been reported only once to our knowledge (E. Gübelin and J.I. Koivula, *Photoatlas of Inclusions in Gemstones*, Vol. 2, Opinio Publishers, Basel, Switzerland, 2005, 829 pp.).

Figure 79. A colorless subhedral forsterite (Fo) inclusion and a dolomite (Dol) inclusion with an unknown dark material attached. Photomicrograph by Jinlin Wu; field of view 0.66 mm.

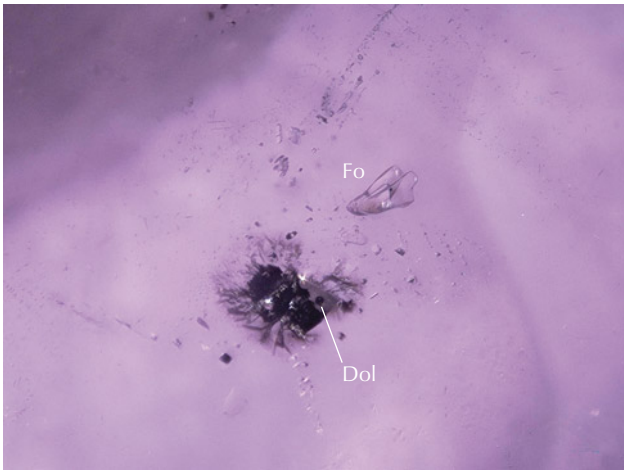

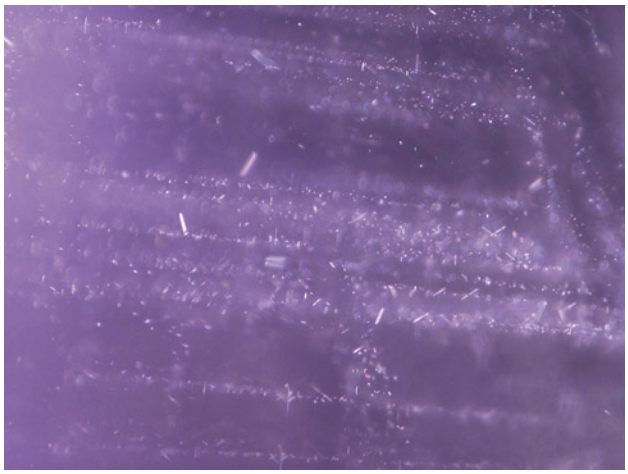

Figure 80. Oriented short needles in the spinel. Photomicrograph by Jinlin Wu; field of view 1.10 mm.

In Tanzania, the primary deposits of spinel occur in marbles and calc-silicate rocks that belong to the Neoproterozoic metamorphic Mozambique Belt (G. Giuliani et al., "Les gisements de rubis et de spinelle rouge de la Ceinture Métamorphique Néoprotérozoıque Mozambicaine," *Revue de Gemmologie*, Vol. 192, 2015, pp. 11–18). Under high-temperature conditions, spinel and forsterite are both stable mineral phases in marbles (Giuliani et al., 2017). Spinel is found in marble or impure marble associated with calcite, dolomite, forsterite, clinohumite, and phlogopite in deposits in Myanmar and Vietnam. Thus, forsterite is commonly seen as an inclusion in spinel from these sources (G. Giuliani et al., "Pink and red gem spinels in marble and placers," *InColor*, No. 43, 2019, pp. 14–28).

It was noteworthy to see forsterite in the Tanzanian sample. This finding could indicate a similar formation environment between spinel in Tanzanian deposits and those in Myanmar and Vietnam.

Jinlin Wu (wujl@ngtc.com.cn), Hong Ma, and Huihuang Li
National Gemstone Testing Center Shenzhen Lab
Shenzhen, China

DIAMONDS

Grayish blue CVD diamond colored by GR1 and SiV⁻. Silicon is a common impurity in chemical vapor deposition (CVD) laboratory-grown diamond. The silicon-related SiV⁻ center, which has zero-phonon lines at 736.6 and 736.9 nm

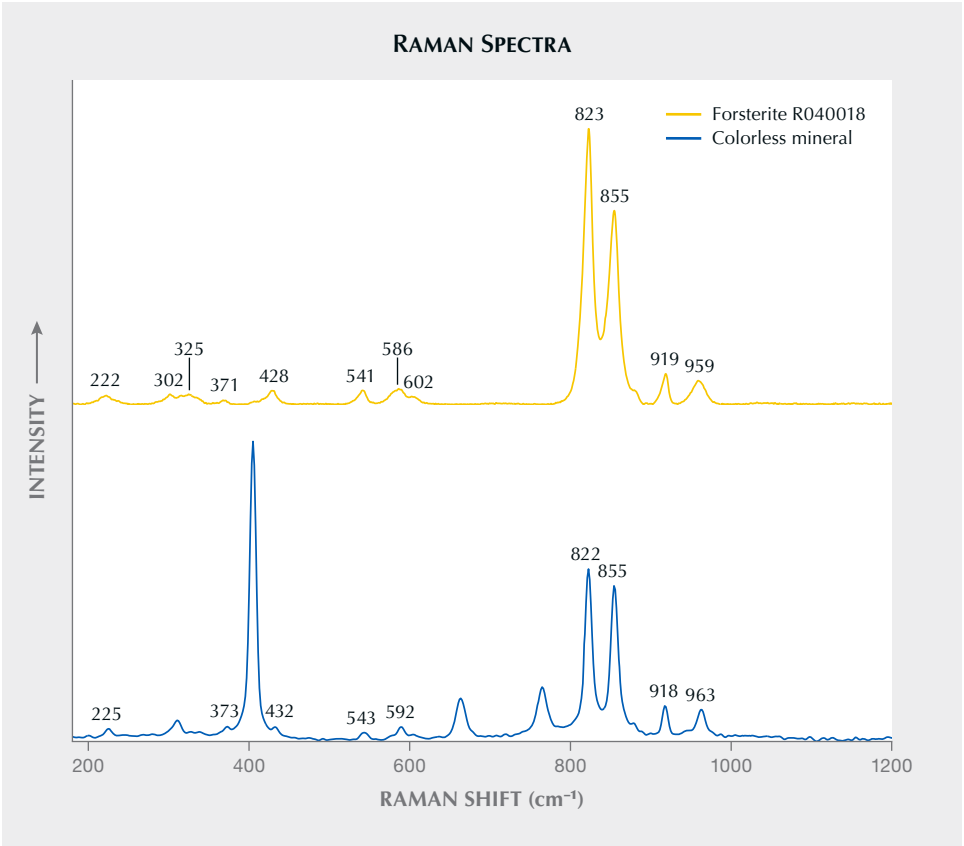

Figure 81. Comparison of Raman spectra of the colorless mineral and forsterite in the RRUFF database. Peaks in the inclusion spectrum at 312, 405, 664, and 766 cm^{-1} are from the host spinel. Spectra are offset vertically for clarity.

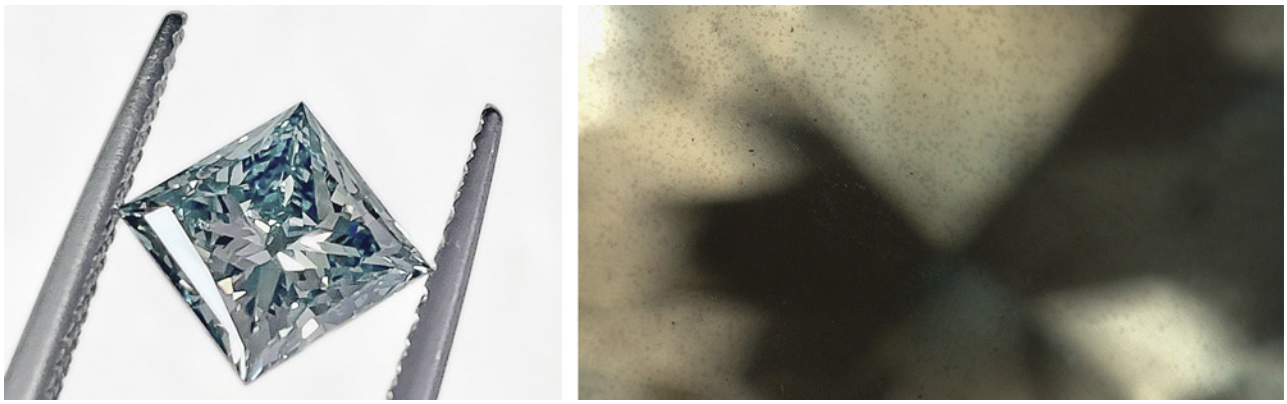

Figure 82. Left: This 1.63 ct grayish blue diamond was identified as a CVD synthetic, with its color caused by both the GR1 and SiV^- centers. Photo by Xiaoyu Zhang. Right: Dark cloud-like non-diamond carbon inclusions. Photomicrograph by Meng Li; field of view 0.25 mm.

and is active in absorption and luminescence, is widely considered an identifying feature of CVD diamond. Generally, the SiV^- center is detected by photoluminescence spectroscopy and is not observed using absorption spectroscopy for most CVD synthetics due to the low silicon content. The absorption spectra may reveal the presence of the SiV^- center in the case of a relatively high silicon content, but rarely in amounts significant enough to affect the color. When the silicon content becomes particularly high, the absorption of SiV^- is in sufficient concentration to influence the bodycolor of a diamond. It has been reported that the color of silicon-doped blue CVD diamonds produced by the PDC Company is attributed to strong absorption of the rather intense SiV^- center (A. Peretti et al., "New generation of synthetic diamonds reaches the market (Part A): Identification of CVD-grown blue diamonds," *Contributions to Gemology*, No. 14, 2013, pp. 3–20).

National Gemstone Testing Center's (NGTC) Beijing laboratory recently received a 1.63 ct grayish blue princess cut (figure 82, left) for identification. Standard testing identified it as a CVD synthetic diamond. The sample showed an even color distribution. Microscopic investigation revealed abundant non-diamond carbon inclusions in the form of both crystals and clouds, with the clouds distributed along the growth layer (figure 82, right). The visible/near-infrared (Vis-NIR) spectrum (figure 83), recorded at liquid nitrogen temperature, included a strong broad SiV^- center defect at 737 nm next to an equally strong GR1 center. The diamond's grayish blue bodycolor was attributed to both the strong GR1 center and the high intensity of the SiV^- center, which produced preferential absorption in the red part of the spectrum. In addition, weak absorptions at 830, 856, and 946 nm (the SiV^0 center) were observed, which were also reported in CVD synthetic

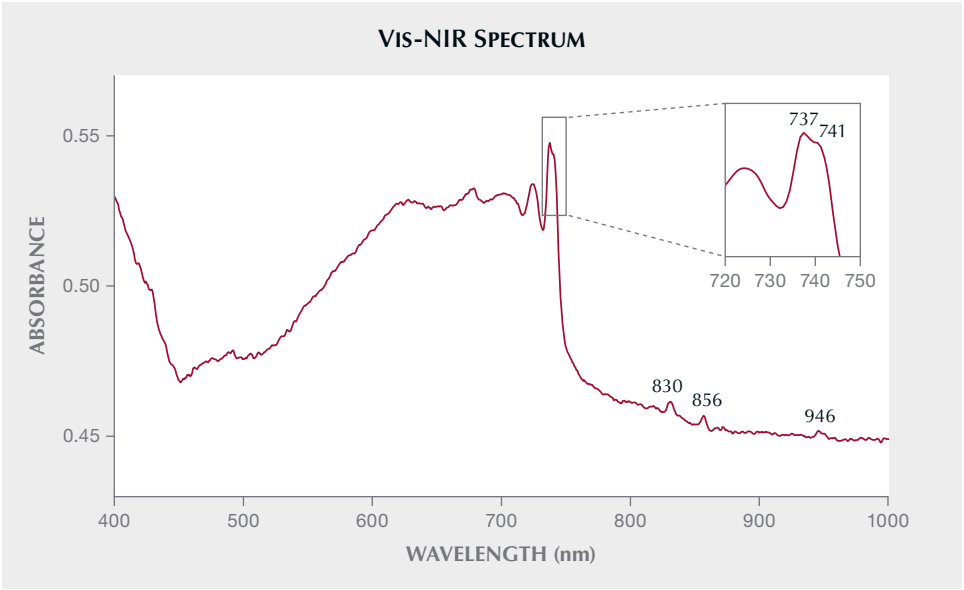

Figure 83. In the Vis-NIR region, in addition to very strong absorptions at 737 nm (SiV^-) and 741 nm (GR1), weak absorptions at 830, 856, and 946 nm (SiV^0) were observed.

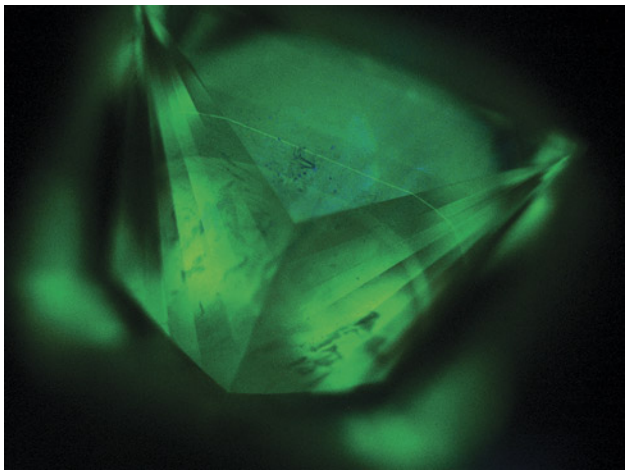

Figure 84. DiamondView imaging showed green fluorescence with blue dislocations. The diamond also revealed a layered growth structure, indicating a start-stop cycling growth process typical of CVD diamond, as CVD diamond growth takes place layer by layer on the top surface of the growing crystal. Image by Xiaoyu Zhang.

diamonds with high silicon content (Peretti et al., 2013; Z. Song et al., "Silicon-doped CVD synthetic diamond with photochromic effect," *Journal of Gems and Gemmology*, Vol. 18, No. 1, 2016, pp. 1–5).

Infrared spectroscopy showed features typical for type IIa diamond (i.e., no defect-related absorptions were detected). The diamond was inert to short-wave and long-wave ultraviolet illumination. Under the ultra-short-wave UV radiation of the DiamondView, the sample fluoresced green, with minor areas showing some blue dislocations. It also showed subtle growth striations and two parallel planes fluorescing stronger than the bulk of the crystal (figure 84). The sample did not phosphoresce. Photoluminescence (PL) spectra taken with various laser excitation wavelengths and at liquid nitrogen temperature (figure 85) showed the presence of radiation-related features including very strong 3H at 503.5 nm, strong GR1 at 741 nm, and weak 486.3 nm. The PL spectra also indicated strong nitrogen-vacancy centers at 575 NV^0 and 637 NV^- nm and multi-nitrogen defects such as H3 and H2, combined with the absence of the unassigned 596/597 nm doublet that is normally seen in as-grown CVD synthetics, suggesting that it had undergone post-growth high-temperature annealing before irradiation.

The PL spectrum with 532 nm laser excitation also exhibited a rather large silicon doublet peak at 736.6/736.9 nm that dwarfs all other PL peaks, including the GR1 in the spectrum. The intensity ratio between the 736.6/736.9 nm PL peak and the diamond Raman peak was about 52. The PL spectrum reaffirmed that the 737 nm absorption peak of the ultraviolet/visible spectrum was the SiV^- defect, and the

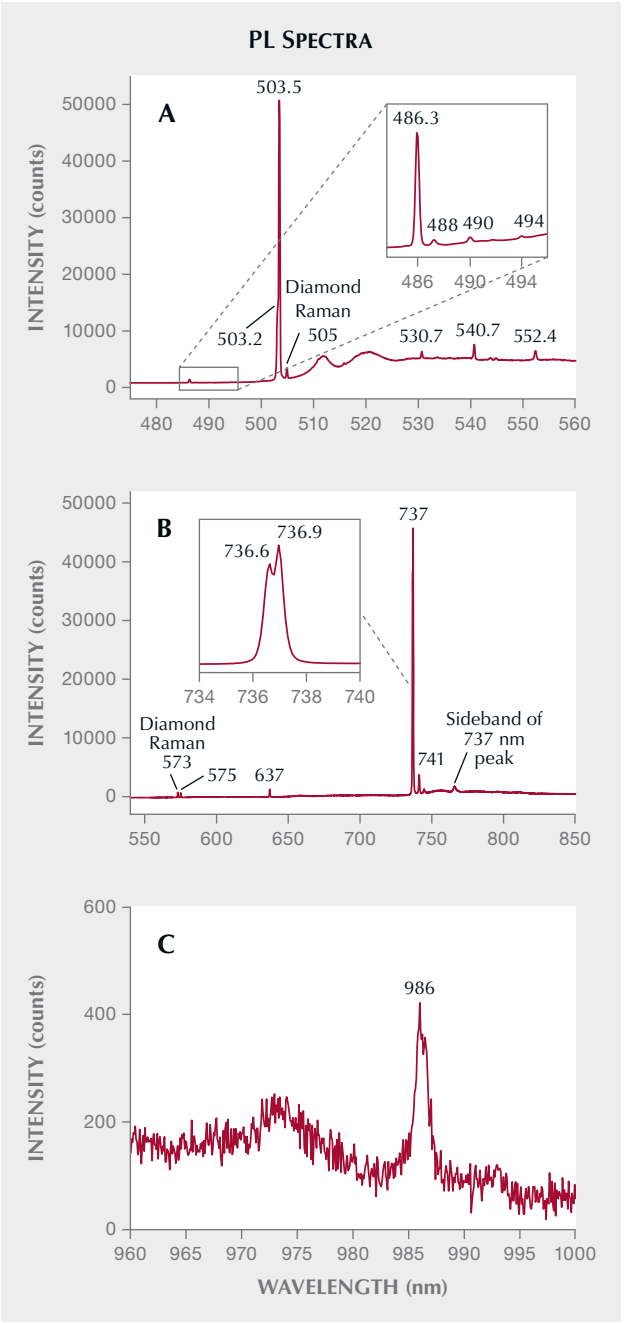

Figure 85. The PL spectrum of the grayish blue CVD synthetic diamond obtained with 473 nm excitation (A) showed that the H3 center (503.2 nm) and radiation-related features included very strong 3H at 503.5 nm and weak 486.3 nm. B: 532 nm excitation revealed the NV centers and silicon-vacancy center that are typically observed in CVD-grown diamonds, along with strong GR1. C: 785 nm excitation showed the H2 center at 986 nm.

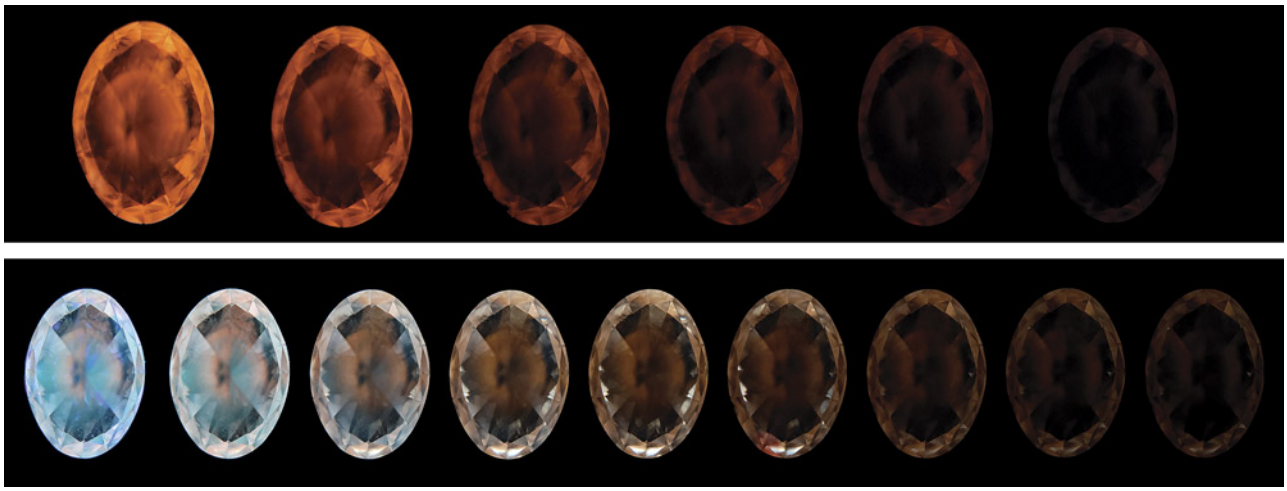

Figure 86. Top: A series of images showing the gradual change (left to right) in the phosphorescence of the 0.71 ct HPHT-grown colorless diamond after removing it from the LWUV source (left image) in increments of 30 seconds for 150 seconds (right image). Bottom: The gradual change in phosphorescence after exposure to a SWUV source (left image) in increments of 30 seconds. The greenish blue and orange emissions decay differently, with the blue fading faster (~90 seconds, fourth image from left) than the orange (~240 seconds, right image). Images by Guy Borenstein.

silicon content of this diamond was so high that it produced strong absorption in the red range of visible light and affected the color of the diamond together with the GR1 center.

Wang Yang (wangyang@ngtc.com.cn), Xiaoyu Zhang, and Zhonghua Song
NGTC, Guangzhou and Beijing

HPHT-grown colorless diamond displaying unusual phosphorescence effects. Phosphorescence longer than 10 seconds in reaction to ultraviolet radiation is regularly observed in colorless to near-colorless and blue-colored diamonds grown by a high-pressure, high-temperature (HPHT) technique. The gemological laboratory of Stuller Inc. recently tested an HPHT-grown colorless (approximately E color grade with a blue-gray overtone) oval brilliant diamond weighing 0.71 ct that showed unusual fluorescence and phosphorescence reactions.

When exposed to a long-wave ultraviolet (LWUV, 365 nm) source for 60 seconds using a standard UV viewing cabinet, the stone emitted a gradually increasing strong orange fluorescence, followed by a long-lasting noticeable phosphorescence (~150 seconds, figure 86, top). The fluorescence and phosphorescence reactions demonstrated a nonuniform color distribution. Similar results were observed using other light sources, including 395 nm UV LED, 405 nm blue laser, a tungsten incandescent flashlight, and a fiber-optic halogen unit.

Given that orange phosphorescence can also be generated by low- and non-UV light sources, further analysis was performed using a series of spectral bandpass filters to identify other wavelengths that stimulate the orange phosphorescence. Testing demonstrated that medium- to strong-intensity light centered at around 430 nm produces the excitation.

Under short-wave ultraviolet (SWUV, 254 nm) radiation using a standard viewing UV cabinet and a De Beers PhosView instrument, the stone displayed a mix of strong greenish blue and medium orange zoned fluorescence and phosphorescence (figure 86, bottom). The colored phosphorescing areas decayed at different rates, with the greenish blue fading faster than the orange (~90 seconds vs. ~240 seconds, with a half-life of about 25 and 35 seconds, respectively).

Deep-UV (<225 nm) imaging demonstrated a strong greenish blue fluorescence with a clear cuboctahedral structure associated with HPHT growth (figure 87). After removal

Figure 87. Deep-UV imaging of the 0.71 ct colorless diamond showing a cuboctahedral-structured luminescence associated with HPHT growth. Image by Guy Borenstein.

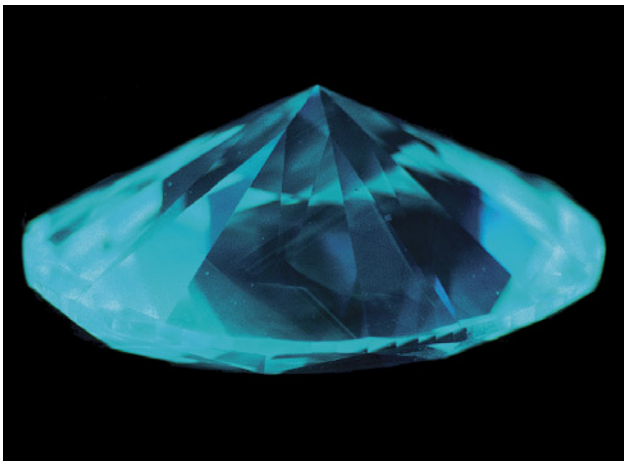

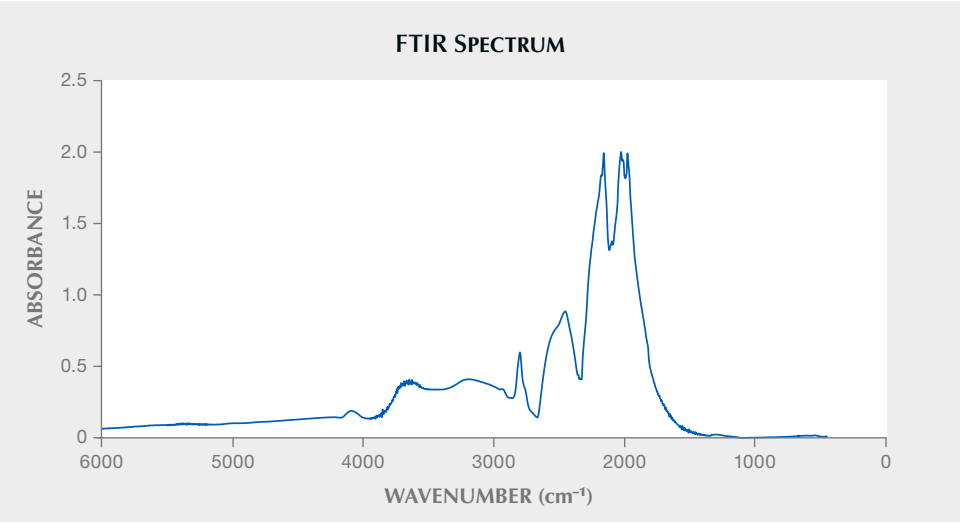

Figure 88. The infrared spectrum of the 0.71 ct HPHT-grown diamond revealed it was type IIb with relatively high levels of uncompensated boron (for a colorless diamond) at 4089, 2929, 2800, and 2455 cm^{-1}.

from the excitation source, the stone displayed a phosphorescence reaction similar to the reaction under SWUV.

Infrared spectroscopy revealed a type IIb diamond with relatively high levels of electrically uncompensated boron at 4089, 2929, 2800, and 2455 cm^{-1} (figure 88). Photoluminescence spectroscopy with 532 nm laser excitation at liquid nitrogen temperature (77K) showed no results, except for the diamond's first- and second-order Raman spectrum peaks, a common tendency in HPHT-grown colorless diamonds (S. Eaton-Magaña et al., "Observations on HPHT-grown synthetic diamonds: A review," Fall 2017 *G&G*, pp. 262–284).

The two phosphorescence colors emitted and their relatively long duration are well-known properties of HPHT-grown diamonds (S. Eaton-Magaña and R. Lu, "Phosphorescence in type IIb diamonds," *Diamond and Related Materials*, Vol. 20, No. 7, 2011, pp. 983–989; Eaton-Magaña et al., 2017), and a blue-orange luminescence combination in one gem was also previously reported (Eaton-Magaña and Lu., 2011; B. Deljanin et al., "NDT breaking the 10 carat barrier: World record faceted and gem-quality synthetic diamonds investigated," *Contributions to Gemology*, Vol. 15, No. 1, 2015) but of weaker intensity. The laboratory-grown diamond's property of bicolor, decay-varying phosphorescence has been previously reported as well (K. Watanabe et al., "Phosphorescence in high-pressure synthetic diamond," *Diamond and Related Materials*, Vol. 6, No. 1, 1997, pp. 99–106; Eaton-Magaña and Lu, 2011; Ulrika F.S. D'Haenens-Johansson et al., "Large colorless HPHT-grown synthetic gem diamonds from New Diamond Technology, Russia," Fall 2015 *G&G*, pp. 260–279).

Considering the HPHT growth method, the long-lasting greenish blue phosphorescence produced by exposure to SWUV and deep UV was expected. It was previously suggested to be related to nitrogen-boron donor-acceptor pair recombination (Watanabe et al., 1997). However, the orange phosphorescence demonstrated a new stimulation source. Its combination with the greenish blue phosphorescence and the identified visible-light excitation wavelength reinforces the theory that the recorded orange phosphorescence is of a different donor-acceptor pairing.

Light of 430 nm wavelength can be found in most fluorescent and all incandescent indoor light sources, as well as the desk lamps and color grading cabinets found in gemological laboratories. Therefore, considering the possibility of more diamonds with this property in the market, their phosphorescence produced from visible light makes it challenging to assign a color in the colorless to near-colorless range for these diamonds during grading. Even under standard non- or low-UV output 6500K fluorescent bulbs, the orange luminescence generated by the source becomes noticeable, adding a yellowish overtone to the blue-gray bodycolor and changing its apparent color grade to approximately F to G. Such a change may impair the diamond grader's ability to accurately assess the stone's bodycolor.

Guy Borenstein and Sean O'Neal
Stuller Inc.
Lafayette, Louisiana

SYNTHETICS AND SIMULANTS

Synthetic color-change wakefieldite. Author AA, a gemstone cutter and collector of rare synthetic gems, recently submitted one rough and one faceted stone to GIA for scientific examination. The material, sourced from RG Crystals in Bangkok, was stated to be Czochralski-pulled, neodymium-doped yttrium orthovanadate, which is commonly used in laser applications. It can also form naturally as the mineral wakefieldite-(Y), with an ideal chemical formula of YVO_4. His first observation was a striking color change from pink or purple to a blue or even green color under various lighting conditions and viewing angles. The finished gemstone (figures 89 and 90) displayed strong fire due to the material's very high dispersion.

Wakefieldite is a rare tetragonal mineral belonging to the xenotime mineral family with an ideal general formula of $(REE)VO_4$, where REE = Y, La, Ce, and Nd among other

Figure 89. Faceted and rough synthetic wakefieldite in LED lighting with 6400K color temperature. The faceted stone is 5.04 ct. Photo by Adriana Gudino; courtesy of Arya Akhavan.

rare earth elements. Its general physical and optical properties include a hardness of 5, specific gravity of 4.25, uniaxial + optic sign with refractive indices of n_ω = 2.000 and n_ε = 2.140, birefringence of 0.140, and dispersion of 0.084. With prominent, perfect cleavage and relatively low hardness, the material is difficult to polish. Natural wakefieldite occurs as very small, non-gem crystals unsuitable for faceting; Czochralski-pulled materials represent the only examples of faceted wakefieldite. In fact, this was the first faceted synthetic wakefieldite seen in a GIA laboratory. Chemistry and visible absorption spectra were collected to quantitatively study the striking color-change behavior.

A polished wafer with 10.6 mm thickness was analyzed. Laser ablation–inductively coupled plasma–mass spectrometry revealed the material was composed of mostly yttrium and vanadium, with 2.2% neodymium by weight (0.03 per

Figure 90. The color change of the faceted synthetic wakefieldite, observed between daylight (left) and cool fluorescent light F10 (right). Photos by Aaron Palke; courtesy of Arya Akhavan.

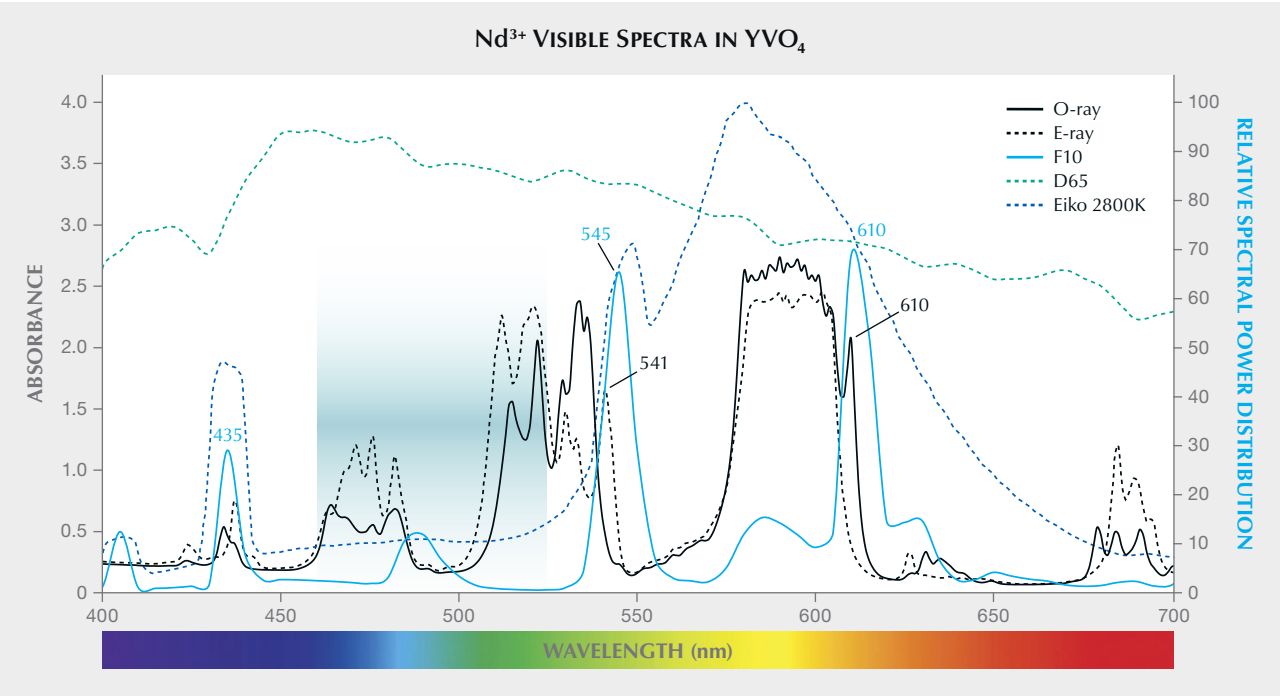

Figure 91. The visible absorption spectra of neodymium-doped YVO_4 are shown with the relative power distribution curves of CIE illuminants F10 and D65 and an Eiko warm white fluorescent bulb with color temperature of 2800K.

formula unit). Since Y^{3+} does not produce color on its own, the color must be derived from the addition of Nd^{3+} ions substituting for Y^{3+} ions in the crystal lattice. Figure 91 shows polarized absorption spectra in the visible range collected with an ultraviolet/visible/near-infrared spectrometer for both the ordinary ray (o-ray) and extraordinary ray (e-ray). The expected color was calculated from the absorption spectra based on the formula described by Z. Sun et al. ("Quantitative definition of strength of chromophores in gemstones and the impact on color change in pyralspite garnets," *Color Research and Application*, Vol. 47, No. 5, 2022, pp. 1134–1154).

As shown in figure 92, the material exhibited a general pink to purple to violet color in most illuminants except the Eiko warm fluorescent light and the o-ray of CIE standard illuminant F10, which represents a typical cool fluorescent light. In fact, the color-change behavior noticed by author AA could be replicated when comparing illuminant F10 to any of the other illuminants such as daylight or incandescent light. Switching between warm incandescent light and actual cool daylight did not produce a dramatic change of color. The emission spectrum of F10 fluorescent light is mainly composed of sharp peaks at 435, 545, and 610 nm (figure 91). Therefore, the color of the synthetic wakefieldite crystal under illuminant F10 is only determined by the small absorption features at ~435, 541, and 610 nm of the Nd^{3+} ions. Broadband emitters such as incandescent light and actual daylight (D65 in figure 91), on the other hand, do not have these sharp emission features, so the color was determined by the transmission windows in the spectrum (440–460, 490–500, 550–570, and 620–670 nm), which remain constant when switching between these illuminants. This was confirmed by observation of the stone in outdoor conditions, which produced the same pinkish purple color seen in incandescent light. The use of warm fluorescent light (Eiko fluorescent light in figures 91 and 92) with color temperature of 2800K also reproduced the greenish blue to blue color seen in cool fluorescent light (F10). It is also worth noting that the absorption features of Nd^{3+} ions at 541 and 610 nm were strongly dependent on the polarization of the light, resulting in a strong pleochroism (grayish purple for the o-ray and green-blue for the e-ray), only observed under F10 illuminant (figure 92).

The color panels under two LED illuminants in GIA's standard viewing box were also calculated in figure 92. The two LED lights, warm and cool, closely imitate the CIE standard illuminants A and D65. The two sets of color panels (A = LED warm pair and D65 = LED cool pair) are extremely close to each other based on their L, C, and H (lightness, chroma, and hue) color coordinates. This study also illustrates the consistent results of GIA's standard viewing box in grading gemstone color.

Ziyin Sun, Shiyun Jin, Adriana Gudino, and Aaron C. Palke
Carlsbad, California

Arya A. Akhavan
Surgical Precision Gems, Toronto

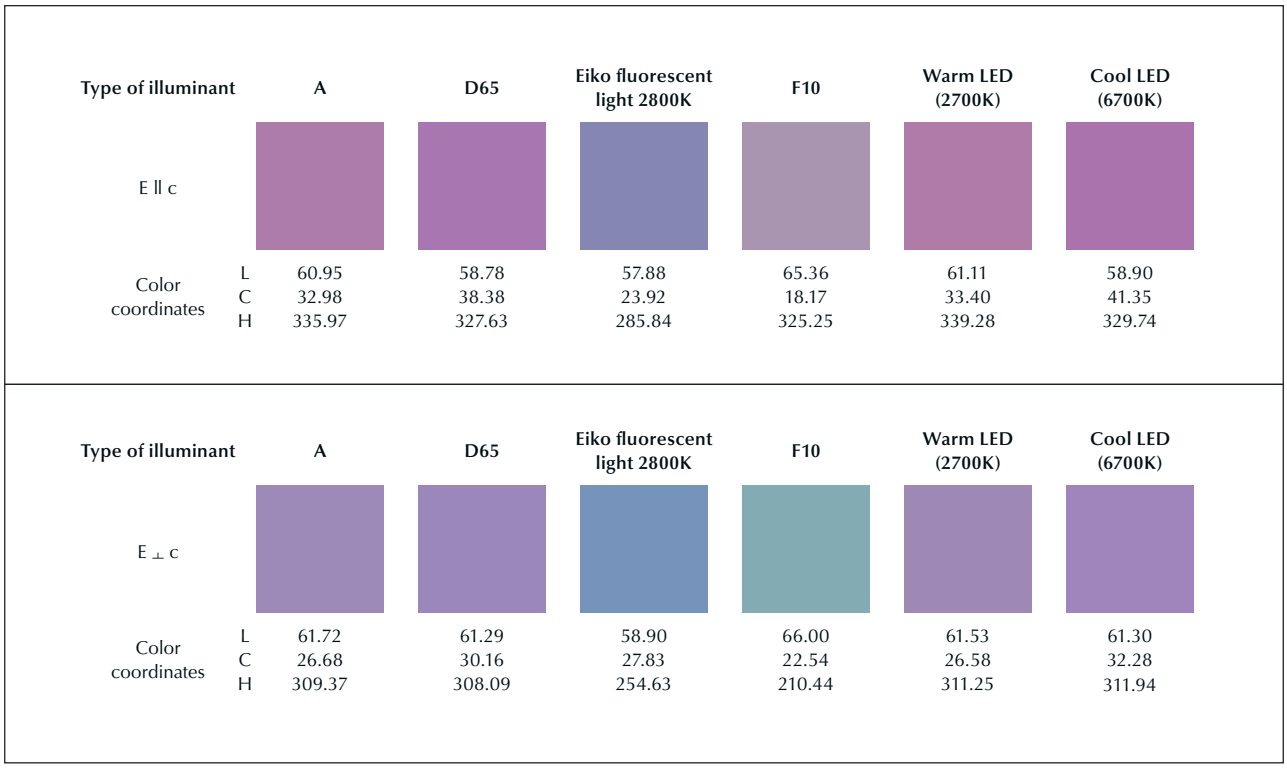

Figure 92. Color panels of the 10.59 mm wafer in six different lighting conditions were calculated for both the o-ray and e-ray. In the top row, A and D65 are CIE standard illuminants for incandescent light and daylight. Eiko is a fluorescent bulb with color temperature of 2800K, while F10 is a CIE standard narrowband fluorescent illuminant. Warm (2700K) and cool (6700K) LEDs represent the illuminants in the GIA standard viewing box.

TREATMENTS

Heated purplish pink sapphire from Ilakaka (Madagascar) with colored monazite inclusions. The Laboratoire Français de Gemmologie (LFG) received a 3.02 ct purplish pink sapphire (figure 93) for identification. Under the microscope, zircon and monazite inclusions (figure 94) along with tubes (figure 95) were observed. This inclusion scene was characteristic of similarly colored sapphires from Ilakaka, Madagascar (W. Wang et al., "The effects of heat treatment on zircon inclusions in Madagascar sapphires," Summer 2006 *G&G*, pp. 134–150; S. Saeseaw et al., "Low-temperature heat treatment of pink sapphires from Ilakaka, Madagascar," Winter 2020 *G&G*, pp. 448–457). No indication of heating was observed. Moreover, the monazite inclusions were orange-brown. It was previously observed that monazite inclusions in pink sapphires turn colorless when heated above 600°C (see again Saeseaw et al., 2020).

Using Raman spectroscopy, the full width at half maximum (FWHM) of the band around 1010 cm^{-1} due to antisymmetric stretching vibration SiO_4 in the zircon structure and the band around 975 cm^{-1} due to PO_4 stretching vibration in the monazite structure can decrease during heating of pink sapphires from Ilakaka (Wang et al., 2006; Saeseaw et al., 2020). The zircon and monazite inclusions were analyzed using a Raman Renishaw inVia spectrometer, with a 514 nm diode-pumped solid-state (DPSS) laser, with about 10 mW laser power on the sample, 50× long working distance objective lens, confocal mode (100 microns entrance slit), 1800 lines/mm grating, and about 1.5 cm^{-1} spectral res-

Figure 93. A 3.02 ct heated purplish pink sapphire measuring 9.57 × 7.74 × 4.55 mm. Photo by Ugo Hennebois.

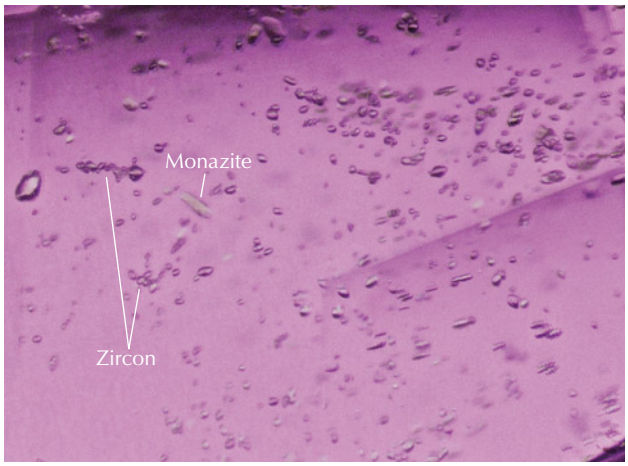

Figure 94. A series of colorless zircon inclusions and orange-brown monazite inclusions in the heated purplish pink sapphire. Photomicrograph by Ugo Hennebois; field of view 1.5 mm.

olution. The FWHM of the most intense band of seven monazite inclusions at around 975 cm^{-1} ranged from 12.7 to 14.2 cm^{-1}, and those of 10 zircon inclusions at around 1010 cm^{-1} ranged from 6.4 to 7.8 cm^{-1}. Both appeared to be sharper and less variable compared to FWHM in unheated pink sapphires, which present zircon inclusions with FWHM of the main band from 7.1 to 21.7 cm^{-1} and monazite inclusions with FWHM of the main band from 14.2 to 18.4 cm^{-1} (Saeseaw et al., 2020; M. Krzemnicki et al., "Zircon inclusions in unheated pink sapphires from Ilakaka, Madagascar: A Raman spectroscopic study," *Proceedings of the Online International Gemmological Conference*, 2021, pp. 21–23; S. Karampelas et al., "Détection du traitement thermique à basse température des corindons," *Revue de Gemmologie a.f.g.*, No. 217, 2022, pp. 4–5).

Unpolarized Fourier-transform infrared spectra in different directions were collected using a Thermo Fisher Magna-IR560 with 4 cm^{-1} spectral resolution and 500 scans using a diffuse reflectance accessory as beam condenser. The sample presented a band at 3309 cm^{-1} and a less intense band at 3232 cm^{-1}, which in pink sapphire is considered an indication of heating (Saeseaw et al., 2020). These bands are linked to different forms of titanium associated with hydroxyl defects in corundum (E. Balan, "Theoretical infrared spectra of OH defects in corundum (α-Al_2O_3)," *European Journal of Mineralogy*, Vol. 32, No. 5, 2020, pp. 457–467).

In line with previous experiments showing that monazite inclusions can keep their color after heating to 600°C (Saeseaw et al., 2020), the presence of colored monazite inclusions alone cannot serve as evidence that a pink sapphire from Ilakaka is unheated. On the other hand, the presence of colorless monazite inclusions in pink sapphires from Ilakaka could be considered an indication of heat treatment.

Ugo Hennebois, Aurélien Delaunay, and Stefanos Karampelas (s.karampelas@lfg.paris)
LFG, Paris

Figure 95. Unaltered tubes in the heated purplish pink sapphire. Photomicrograph by Ugo Hennebois; field of view 2 mm.

Chromophore behaviors (including the 880 nm absorption band) in an irradiated pink sapphire. Irradiation is a known process for enhancing color in corundum, particularly yellow and pink sapphire. Recently, some rubies and pink sapphires with bluish tint were reportedly treated with radiation ("LMHC makes progress on laboratory report harmonisation, discussed current challenges in detection of corundum treatments," LMHC press release, March 14, 2023). However, chromophore behaviors in irradiated ruby/pink sapphire have not been fully investigated. This report shows preliminary results of an experiment involving irradiated pink sapphire. An untreated Madagascar pink sapphire with a blue modifier (figure 96) was fabricated as an optical wafer with two polished faces perpendicular to the *c*-axis for ultraviolet/visible/near-infrared (UV-Vis-NIR) spectroscopic study. Trace element chemistry was analyzed in the UV-Vis-NIR measurement area using laser ablation–inductively coupled plasma–mass spectrometry. This information can be used to link the visual color and the color-causing trace elements listed in figure 96.

The spectrum of the untreated sample displayed broad absorption bands at ~400 and ~560 nm together with weak peaks at ~470 and at 693 nm, demonstrating that the Cr^{3+} chromophore was responsible for the pink color (blue line in figure 97; see E.V. Dubinsky et al., "A quantitative de-

Elements	Mg	Ti	V	Cr	Fe	Ga
Concentration (ppma)	30 ± 7[a]	21 ± 4	16 ± 1	137 ± 7	480 ± 27	15 ± 1
Detection limits (ppma)	0.05	0.14	0.01	0.17	2.2	0.01

[a]*average ± standard deviation*

Figure 96. Color-calibrated photo of a 0.664 ct pink sapphire from Madagascar before and after irradiation, and after fade test using fiber-optic light for 6 hours. Path length/thickness: 1.514 mm. Photos by Sasithorn Engniwat.

scription of the causes of color in corundum," Spring 2020 *G&G*, pp. 2–28). This sample also showed a weak broad band at around 580 nm related to Fe^{2+}-Ti^{4+} pairs, which produced a blue color, modifying the pink color from Cr^{3+} to purple-pink. Weak Fe^{3+}-related absorption features were also observed, represented by a broad band at ~330 nm and narrow peaks at 377, 388, and 450 nm. The iron-related chromophore only causes significant yellow color at relatively high iron concentrations (greater than ~1000 ppma) due to Fe^{3+} chromophores' weak color strength.

For our radiation experiment, the sample was treated with a gamma irradiation dose of 500 kGy at the Irradiation Center at the Thailand Institute of Nuclear Technology (public organization). After irradiation, the pink sapphire changed to a padparadscha-like coloration in which the subtle blue color was partially removed (figure 96). The UV-Vis-NIR spectrum after irradiation showed a significant increase in absorption intensities at wavelengths shorter than ~560 nm or longer than ~660 nm (red line in figure 97). To observe changes in chromophore be-

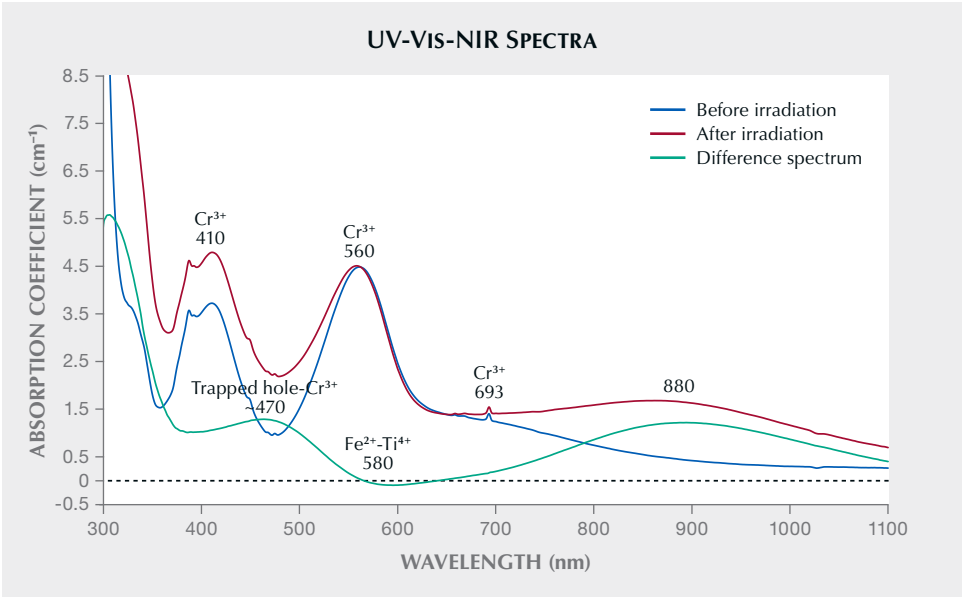

Figure 97. Polarized UV-Vis-NIR spectra comparisons of the pink sapphire before and after irradiation with a gamma irradiation dose of 500 kGy. The difference spectrum revealed a significant increase in trapped hole paired with Cr^{3+} and the 880 nm band in the irradiated pink sapphire.

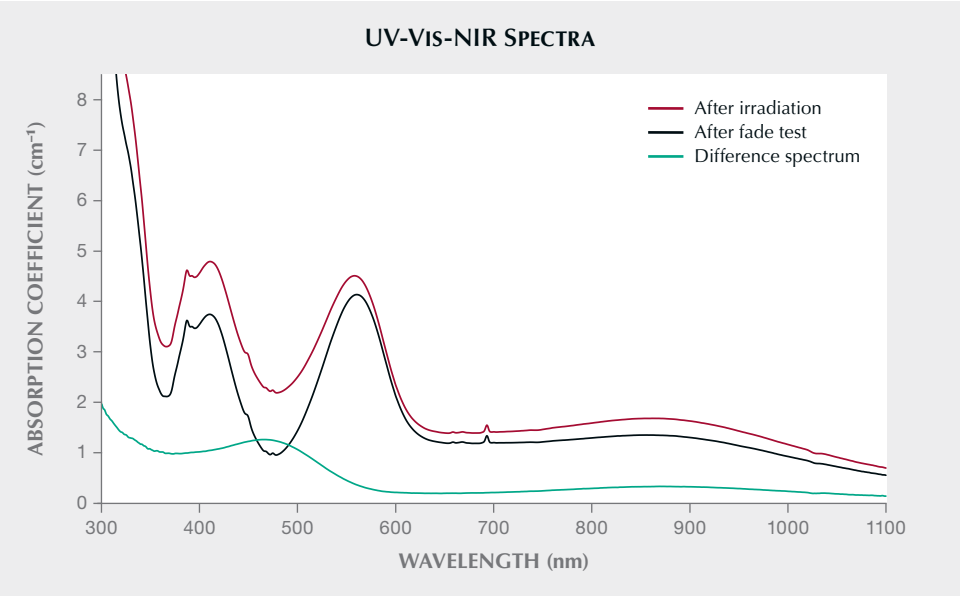

Figure 98. Polarized UV-Vis-NIR spectra comparisons of the pink sapphire after irradiation with a gamma irradiation dose of 500 kGy and after the fade test. The difference spectrum between after irradiation and after fade test obviously shows the reduction in the trapped hole paired with Cr^{3+} chromophore when exposed to intense light for several hours.

havior caused by irradiation, the spectrum after irradiation was subtracted from the pretreatment spectrum. The difference spectrum (green line in figure 97) revealed that this acceptor-dominated corundum with an atomic concentration of magnesium greater than the sum of titanium and silicon concentrations created a strong absorption feature below ~560 nm to the UV region, which matches well with the trapped hole associated with the Cr^{3+} spectrum for causing orange coloration (Dubinsky et al., 2020). Using the absorption cross section information provided in Dubinsky et al. (2020), the concentration of trapped hole-Cr^{3+} chromophores induced by irradiation was approximately 0.8 ppma in the sample. This chromophore had very high color strength, and therefore a noticeable color change could be observed with only a tiny concentration of the trapped hole paired with Cr^{3+} created after treatment. The Fe^{2+}-Ti^{4+} chromophore also reduced by approximately 0.7 ppma in the treated sample, resulting in less blue color modification. This slight lightening in blue color after irradiation is possibly due to the change in oxidation state of iron (which would reduce the number of Fe^{2+}-Ti^{4+} pairs). In addition, the creation of orange color (trapped hole-Cr^{3+}) masked a certain portion of remaining blue color after treatment, as blue and orange are complementary colors. The change in UV-Vis-NIR spectrum corresponded with the change in color appearance caused by irradiation.

When studying absorption features in the UV-Vis-NIR spectrum of corundum, a broad band centered at around 880 nm in the red to near-infrared region is typically associated with basalt-related blue sapphire (e.g., A.C. Palke et al., "Geographic origin determination of blue sapphire," Winter 2019 *G&G*, pp. 536–579). This band has little or no impact on color. In addition to basalt-related blue sapphires that are exposed to heat naturally, the 880 nm band can be induced in the spectrum of a metamorphic-type sapphire that has been heat treated, such as heated Madagascar sapphire (E.B. Hughes and R. Perkins, "Madagascar sapphire: Low-temperature heat treatment experiments," Summer 2019 *G&G*, pp. 184–197) or heated Rock Creek sapphire (J.L. Emmett and T.R. Douthit, "Heat treating the sapphires of Rock Creek, Montana," Winter 1993 *G&G*, pp. 250–272). This feature can also be found in Mozambican ruby after heat treatment (S. Saeseaw et al., "Update on "low-temperature" heat treatment of Mozambican ruby: A focus on inclusions and FTIR spectroscopy," *GIA Research News*, April 30, 2018). The origin of this band is not fully understood but may be related to iron clusters.

The 880 nm band was absent in the UV-Vis-NIR spectrum of this sample before treatment. Interestingly, this pink sapphire developed the 880 nm band after irradiation, with a significant intensity around 1.2 cm^{-1}. Color stability testing is usually performed in gem laboratories for yellow to padparadscha sapphires that may contain unstable color centers (e.g., A.C. Palke et al., "An update on sapphires with unstable color," *GIA Research News*, December 12, 2022; Summer 2022 GNI, pp. 259–260). After the color stability test (figures 96 and 98), the orange coloration introduced by irradiation faded away after exposure to intense incandescent light due to the dissociation of the trapped hole paired with Cr^{3+}, whereas the 880 nm band remained. This preliminary observation suggests that the 880 nm band can be produced by an irradiation process, and this feature could provide some interesting evidence of treatment, either heat or irradiation, in pink sapphires and rubies. However, further studies would be needed to understand the development of the 880 nm absorption band.

Wasura Soonthorntantikul and Wim Vertriest
GIA, Bangkok
Aaron Palke
GIA, Carlsbad